J. Fluid Mech. (2000), *vol.* 406, *pp.* 247–279. Printed in the United Kingdom

Turbulent transport of momentum and heat in magnetohydrodynamic rectangular duct flow with strong sidewall jets

By ULRICH BURR[1]†, L. BARLEON[1], U. MÜLLER[1] AND A. TSINOBER[2]

[1] Forschungszentrum Karlsruhe, Institut für Angewandte Thermo- und Fluiddynamik, Postfach 3640, 76021 Karlsruhe, Germany

[2] Department of Fluid Mechanics and Heat Transfer, Faculty of Engineering, Tel Aviv University, Ramat Aviv, 69978 Tel Aviv, Israel

(Received 17 August 1998 and in revised form 28 October 1999)

This paper presents an experimental study of the momentum and heat transport in a turbulent magnetohydrodynamic duct flow with strong wall jets at the walls parallel to the magnetic field. Local turbulent flow quantities are measured by a traversable combined temperature-potential-difference probe. The simultaneous measurements of time-dependent velocity and temperature signals facilitates the evaluation of Reynolds stresses and turbulent heat fluxes. Integral quantities such as pressure drop and temperature at the heated wall are evaluated and compared with results from conservative design correlations. At strong enough magnetic fields the destabilizing effect of strong shear generated at the sidewalls wins the competition with the damping effect by Joule's dissipation and turbulent side layers are created. Due to the strong non-isotropic character of the electromagnetic forces, the turbulence structure is characterized by large-scale two-dimensional vortices with their axis aligned in the direction of the magnetic field. As most of the turbulent kinetic energy is concentrated in the near-wall turbulent side layers, the temperatures at the heated wall are governed by the development of the thermal boundary layer in the turbulent flow.

1. Introduction

This study has been motivated by the design work of self-cooled liquid-metal fusion blankets where circulating liquid metals such as lithium or a lithium-lead alloy are considered as a coolant and as a breeder material. As the flow of the electrically well-conducting fluid within the blanket is exposed to the strong magnetic field confining the fusion plasma, electric currents are induced in the fluid. The interaction of these currents with the applied magnetic field introduces Lorentz forces to the momentum balance of the flow and a magnetohydrodynamic (MHD) flow is established in the blanket channels.

Although under blanket conditions intense volumetric heat sources caused by γ-radiation and Joule's dissipation are present, the high heat flux at the plasma-facing wall is the central issue of the heat transfer because it determines the temperature at the heat-loaded plasma-facing first wall that has to be kept within acceptable

† Present address: Institut für Hydromechanik und Wasserwirtschaft, Eidgenössische Technische Hochschule Zürich, ETH Hönggerberg, CH-8093 Zürich.

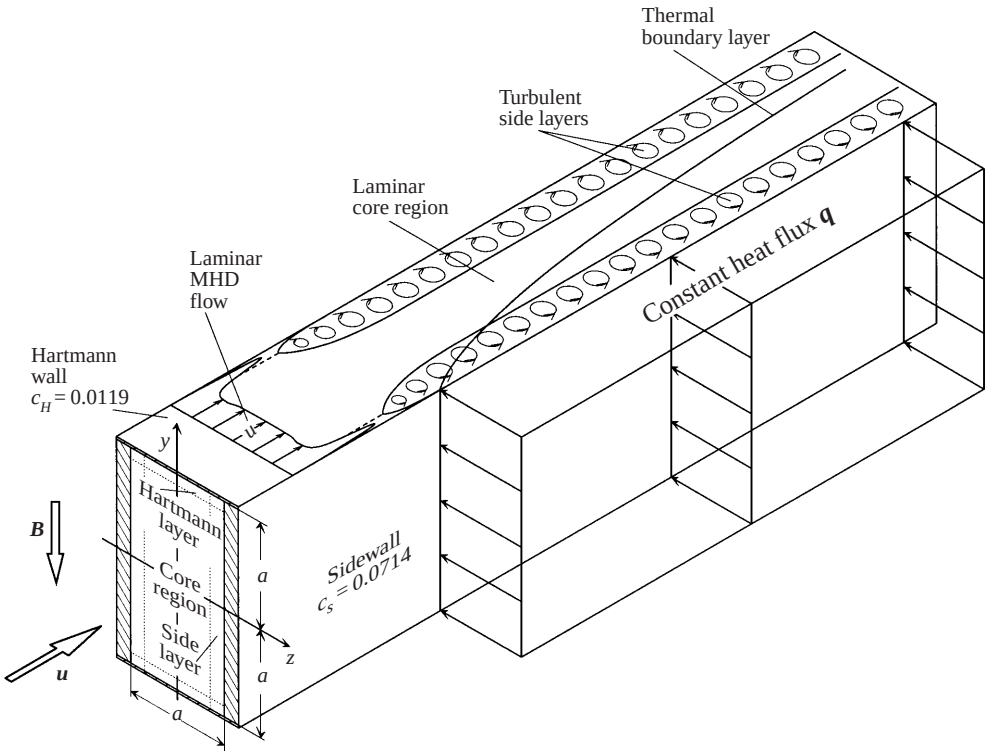

FIGURE 1. Geometry and coordinates of the investigated heat transfer problem. The flow pattern expected in the midplane at $y = 0$ is projected onto the upper Hartmann wall.

limits defined by material properties. For a fundamental study, blanket conditions are simplified to the heat transfer problem schematically illustrated in figure 1.

A constant surface heat flux $\boldsymbol{q}$ is applied to one wall of a straight rectangular duct of an aspect ratio 2 : 1 and removed by a liquid metal MHD flow of velocity $\boldsymbol{u}$. The heated wall belongs to the part of the walls that are oriented parallel to the applied magnetic field $\boldsymbol{B}$ called the sidewalls. The walls perpendicular to the magnetic field are called the Hartmann walls. The boundary layers developing along the duct walls are called side layers and Hartmann layers, respectively. The walls are considered to be thin and of finite electrical conductivity. Conducting properties are expressed by the non-dimensional wall conductance ratios c_H and c_S of Hartmann and sidewalls defined as

$$c = \frac{\sigma_W s}{\sigma a}, \tag{1.1}$$

where σ_W and σ are the electrical conductivities of the wall material and the fluid, s is the thickness of the duct wall considered and a the characteristic length of the duct, i.e. the half-width of the square duct in the direction of the magnetic field. As high flow velocities are required for reliable heat removal, the convective–diffusive heat transfer in the blanket is governed by developing thermal boundary layers.

In the range of fusion-relevant strong magnetic fields, the Lorentz and pressure forces dominate the momentum balance of the flow and cause strong electromagnetic damping by Joule's dissipation. As this MHD dissipation damps out motion on a short time scale of $\tau_{JD} \sim \rho/\sigma B^2$ depending on the magnitude of magnetic induction B, the density ρ and the electrical conductivity of the fluid σ (see Shercliff 1965), turbulent

velocity fluctuations are expected to vanish very fast. Thus, MHD research in channel flows has been frequently focused on stationary inertialess assumptions related to laminar flow. Although the velocity distributions and the pressure drop are sometimes well represented by such asymptotic solutions, turbulent velocity fluctuations have been observed in many experiments. Their existence may be of crucial importance for the removal of heat from high-heat-loaded walls. Heat transfer based on laminar flow requires high flow velocities which may lead to technically unacceptable pressure losses. If turbulent heat transport can be taken into account, the required flow rate may be reduced and the lower pressure drop may lead to simpler technical designs.

The structure of the paper is as follows:

In § 2 the governing equations, their scaling and the non-dimensional numbers are outlined. In § 3 some basic phenomena of turbulent MHD flows in rectangular ducts and general aspects of heat transfer are discussed. The experimental setup is explained in § 4 with particular emphasis on the use of potential probes to obtain local turbulent flow quantities. The experimental results of the isothermal flow are presented in § 5. There the onset of turbulence and its structure is considered and the effect of this special kind of turbulence on the time-averaged flow is discussed. The influence of turbulent mixing on the temperature field is elaborated in § 6 from measurements in which a heat flux is applied to one of the sidewalls.

2. Governing equations and relevant dimensionless groups

Many MHD flows in technical applications are well described by the limiting case of small magnetic Reynolds numbers $Rm \ll 1$ with $Rm = \mu\sigma v_0 a$ representing the ratio of the magnetic field induced by the fluid motion to the externally applied magnetic field. Here, v_0 is the characteristic velocity, i.e. the mean velocity of the duct flow, and μ is the magnetic permeability. In this case the isothermal, non-buoyant flow of the Newtonian fluid is governed by the following set of inductionless equations for conservation of mass, momentum and charge:

$$\nabla \cdot \boldsymbol{v} = 0, \tag{2.1}$$

$$\frac{\partial \boldsymbol{v}}{\partial t} + (\boldsymbol{v} \cdot \nabla)\boldsymbol{v} = -\nabla p + \frac{1}{Re}\Delta \boldsymbol{v} + N\boldsymbol{j} \times \boldsymbol{B}, \tag{2.2}$$

$$\nabla \cdot \boldsymbol{j} = 0, \tag{2.3}$$

and by Ohm's law for moving media

$$\boldsymbol{j} = -\nabla\phi + \boldsymbol{v} \times \boldsymbol{B}. \tag{2.4}$$

In these equations $\boldsymbol{v} = (u, v, w)$, $\boldsymbol{j} = (j_x, j_y, j_z)$, $\boldsymbol{B} = (b_x, b_y, b_z)$, ϕ, t and p denote the non-dimensional velocity, current density, magnetic field, electric potential, time and pressure, scaled with v_0, $\sigma v_0 B$, B, $a v_0 B$, τ_0 and ρv_0^2. The time scale is defined by the advection time of the duct flow calculated from the characteristic velocity and length scale as $\tau_0 = a/v_0$. In addition a characteristic frequency f_0 based on the characteristic time scale is obtained by $f_0 = v_0/a$.

The Reynolds number is given as

$$Re = \frac{a v_0}{\nu} \tag{2.5}$$

and denotes the ratio of inertial and viscous forces in the momentum equation with

the kinematic viscosity v. The interaction parameter

$$N = \frac{\sigma a B_0^2}{\rho v_0} \tag{2.6}$$

represents the ratio of inertia and electrodynamic forces. The product NRe gives the square of the Hartmann number

$$M = aB\left(\frac{\sigma}{\rho v}\right)^{1/2} \tag{2.7}$$

that governs the flow at laminar, fully developed conditions by the balance between viscous and Lorentz forces.

Neglecting volumetric heat sources, the distribution of the non-dimensional temperature T in the flow is determined by the equation

$$\frac{\partial T}{\partial t} + (\boldsymbol{v}\cdot\nabla)T = \frac{1}{Pe}\Delta T. \tag{2.8}$$

The dimensionless temperature T is associated with the dimensional one T^* as $T = (T^* - T_i)/\Delta T$ with the mean temperature at the entrance of the heated section T_i as a reference and a temperature difference $\Delta T = qa/\lambda$ given by the magnitude of the wall heat flux q and the thermal conductivity λ of the fluid. The ratio of convective and diffusive heat fluxes is given by the Péclet number

$$Pe = \frac{v_0 a}{\kappa}, \tag{2.9}$$

where κ is the thermal diffusivity defined as $\kappa = \lambda/\rho c_p$ with the specific heat capacity c_p.

Introducing Reynolds decomposition of the flow variables, e.g. $\boldsymbol{u} = \overline{\boldsymbol{u}} + \boldsymbol{u}'$ and $T = \overline{T} + T'$, with the mean parts denoted by an overbar and the fluctuating parts denoted by a prime, into equations (2.1)–(2.4) and (2.8) and averaging in time one obtains the mean flow equations of mass, momentum, charge and heat. These equations contain additional contributions from the non-vanishing correlations between fluctuations $\boldsymbol{u}'$ and T', namely $-\nabla\overline{\boldsymbol{u}'\boldsymbol{u}'}$ in the momentum equation and $-\nabla\overline{\boldsymbol{u}'T'}$ in the temperature equation. Appropriate knowledge of these quantities is crucial for dealing with any turbulent flow in general and for the development of valid turbulence models for MHD flows in particular. So apart from determining integral flow quantities like the pressure drop and the temperatures at the heated wall this paper is focused on the determination of Reynolds stresses $\overline{\boldsymbol{u}'\boldsymbol{u}'}$ and turbulent heat fluxes $\overline{\boldsymbol{u}'T'}$ as well as on some other properties of the fluctuating part of the flow with particular emphasis on the wall region.

3. Some basic phenomena

3.1. *MHD turbulence in rectangular ducts*

MHD flows in rectangular ducts with conducting walls are characterized by two jet-like shear layers along the sidewalls of the duct parallel to the magnetic field and a core region with almost constant velocity. Figure 2(a) shows a typical laminar velocity distribution in a rectangular duct obtained from an asymptotic solution. As illustrated by the velocity distribution in the midplane of the duct in figure 2(b) an increase of the intensity of the applied magnetic field or M, respectively, causes the jet velocity to increases as $M^{1/2}$, whereas the width δ of the wall jets decreases as $M^{-1/2}$. The enhanced shear of order M in the jet is capable of producing turbulent velocity

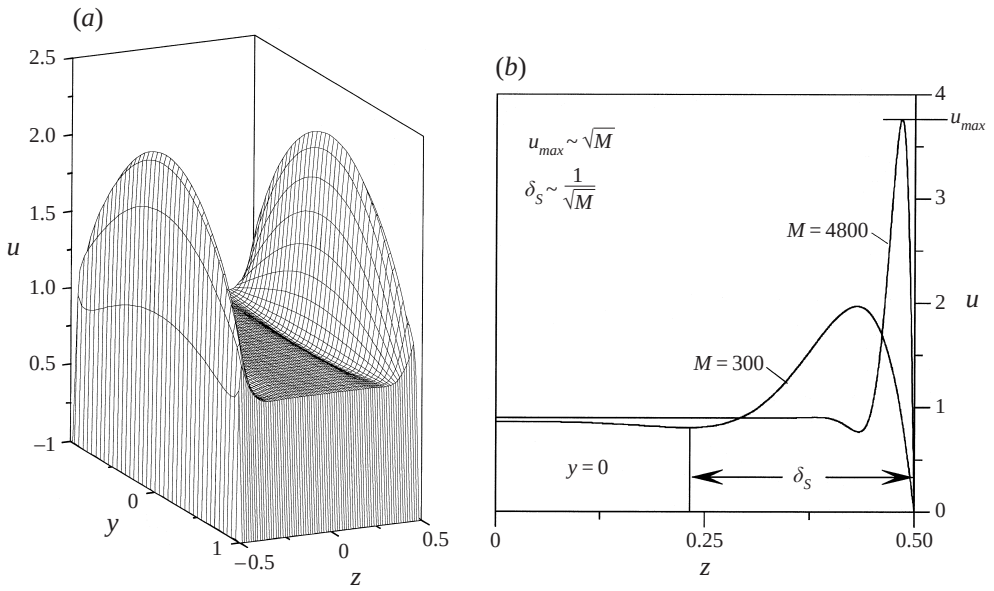

FIGURE 2. Distribution of non-dimensional laminar velocity in a fully developed MHD rectangular duct flow of ascpect ratio 1 : 2, obtained from an asymptotic solution. The wall conductance ratios are $c_H = 0.0119$ for both Hartmann walls and $c_s = 0.0714$ for both sidewalls. (*a*) Three-dimensional distribution at $M = 600$. (*b*) The effect of increasing the Hartmann number from $M = 300$ to $M = 4800$ illustrated by the velocity distributions in the midplane ($y = 0$).

fluctuations even if the flow rate is maintained constant. No mechanical or electrical turbulence promoters are required in such a case. The turbulence promoting effect of the magnetic field in terms of shaping the velocity profile is opposed by Joule's dissipation which is also increasing with the intensity of the magnetic field. A linear stability analysis by Ting *et al.* (1991) yields that in the range of high magnetic fields both effects oppose each other and the critical flow rate becomes independent of the intensity of the applied magnetic field.

At first sight the strong electromagnetic damping of time-dependent turbulent motion seems to make a significant improvement of heat transfer by turbulent transport impossible, but one has to realize on the other side that the Lorentz force has a strong non-isotropic character. Turbulent velocity fluctuations in the direction of the magnetic field decrease quickly by the effect of strong Joule's dissipation whereas turbulent fluctuations in the plane perpendicular to the direction of the magnetic field are only weakly damped. This anisotropic feature leads to the formation of extended vortex tubes oriented parallel to the applied magnetic field provided that the strength of the applied magnetic field is high enough and inertial forces do not further destabilize the flow.

This tendency of vortices in MHD flows to evolve into increasingly two-dimensional vortex columns aligned with the magnetic field was described by Davidson (1995) in the limit case of high Reynolds numbers and small magnetic Reynolds numbers. Concerning axisymmetric, isolated vortices evolving in both space and time in an otherwise quiescent fluid he finds that the component of angular momentum aligned with the magnetic field is conserved whereas components non-aligned with the magnetic field are removed on a fast time scale. The Lorenz force elongates vortices along the field lines and thereby Joule's dissipation is continuously reduced.

Scaling the decay time of isotropic turbulence in MHD flows defined as $\tau_{JD} = \rho/\sigma B^2$ (see § 1) with the eddy turnover time $\tau_{TO} = l/v_0$ as a characteristic time scale for the vortex motion gives the non-dimensional decay time of turbulence

$$\tau^*_{JD} = \frac{1}{N_l}, \tag{3.1}$$

which proves to be the inverse of an interaction parameter $N_l = \sigma l B_0^2/\rho v_0$ based on the characteristic length scale l of the turbulence structure. If N_l becomes small the momentum equation asymptotes towards the hydrodynamic balance. If on the other hand N_l is large, disturbances of the flow decay on a fast time scale. Provided that the fluctuating part of the velocity in forced turbulence is independent of the length scale, the damping of isotropic turbulence increases with the size of the eddies and therefore higher isotropy is expected in the small turbulence scales. However, small eddies are damped by viscosity on a time scale $\tau_V = l^2/\nu$. The ratio of the eddy turnover time to the viscous time scale is

$$\tau^*_V = Re_l, \tag{3.2}$$

the Reynolds number based on the characteristic length of the eddy.

If we restrict ourselves to situations where Re_l is large and N_l is moderate or large, an isolated vortex can be considered as approximately inviscid. An initially three-dimensional disturbance will then evolve into an increasingly two-dimensional structure in the sense that the velocity distribution becomes uniform in the direction of the magnetic field.

In the range of large interaction parameters Sommeria & Moreau (1982) have described the tendency of turbulent structures to extend in the direction of magnetic field lines, as a preferred electromagnetic diffusion process of vorticity $\boldsymbol{\omega} = \nabla \times \boldsymbol{v}$ in this particular direction. In the limit $Rm \ll 1$ it is characterized by a diffusivity $\alpha = \sigma B_0^2 l_\perp/\rho$, based on the length scale $l_\perp$ perpendicular to the magnetic field of the eddy, which renders differences in the velocity of two transverse planes of distance d apart to be equalized on a time scale $\tau_D \approx (\rho/\sigma B_0^2)(d^2/l_\perp^2)$.

If the magnetic forces act for long enough time any differences in the velocity distribution along the direction of magnetic field are removed and a pure two-dimensional turbulent flow is established provided that this is consistent with the boundary conditions. The possibility of creating two-dimensional turbulence in strong magnetic fields was conjectured by Kit & Tsinober (1971); for a review of later developments, see Tsinober (1990) and for more recent results Oughton, Priest & Matthaeus (1994) and Zikanov & Thess.

In purely two-dimensional flow the effect of a magnetic field is reduced to maintaining the two-dimensionality but the flow itself is governed by two-dimensional hydrodynamics. However, in duct flows no-slip conditions at walls have to be satisfied. The diffusion of vorticity along magnetic field lines leads to a uniform velocity distribution along the magnetic field in the core and to the formation of Hartmann layers at the Hartmann walls. The existence of such quasi-two-dimensional (Q2D) turbulent MHD flow has been demonstrated by Platnieks (1972) and Kolesnikov & Tsinober (1972*a*). In Q2D flows, the Hartmann layers and the conducting Hartmann walls offer an additional path for the electric currents induced in the core region, because the induced electric potential is smaller due to the reduced circulating motion. The electromagnetic forces induce in this case the dissipation of kinetic energy from the core region by Joule's dissipation in the Hartmann walls and Joule's and viscous dissipation in the Hartmann layers. The time scale for this process, called Hartmann

braking, is given by Sommeria & Moreau (1982) for insulated Hartmann walls. Bühler (1996) extended the theory of Hartmann braking to thin conducting Hartmann walls of conductivity c_H and derives the expression

$$\tau_H^* = \left(\frac{N_{l_\perp}}{M} + \frac{c_H N_{l_\perp}}{1 + c_H} \right)^{-1}, \tag{3.3}$$

where the current path in the wall is represented by the second term in the brackets. If τ_H^* is moderate or large, the turbulent motion of the Q2D turbulent flow is only weakly damped and a vortex may exist for several turnover times, even when it is not driven by shear. Thus with the parameter τ_H^* it can be estimated whether regions with no shear remain laminar or whether turbulence can penetrate them. The Hartmann braking of eddies was used by Kolesnikov & Tsinober (1972*b*) in experiments investigating the flow behind a cylinder.

The generation of turbulence in the jet-like shear layers of MHD rectangular duct flow at high Hartmann numbers ($2900 < M < 5400$) was investigated first by Reed & Picologlou (1989). They obtained information on the streamwise velocity component in the channel midplane by a traversable potential probe. Above a critical Reynolds number of $2650 < Re_{crit} < 5100$, large velocity fluctuations u' of the order of the mean flow $\bar{u}$ have been observed in the near-wall jet regions whereas the flow in the core region remains laminar. Although the width of the turbulent side layer δ_S was not directly measured, they suggested a scaling law $\delta_S = a/N^{1/3}$. The turbulence observed is distinguished from ordinary hydrodynamic (OHD) turbulence by its regular time structure and its lack of small-scale structures.

3.2. *Heat transfer*

Only a few studies of developing thermal boundary layers in turbulent MHD flows have been carried out up to now, see e.g. Sukoriansky & Branover (1988), Barleon *et al.* (1996) and Evtushenko *et al.* (1995), and the present state of research is far from being satisfactory. For instance Kirillov, *et al.* (1995) have estimated the temperature at the heated wall in the region of developing thermal boundary layers from a boundary layer solution for the temperature assuming laminar slug flow. At constant wall heat flux the non-dimensional temperature at the wall–fluid interface T_W increases as

$$T_W = 2(\zeta/\pi)^{1/2}, \tag{3.4}$$

where $\zeta = x/Pe$ is the thermal developing length of the flow starting at the beginning of the heated section. With the formation of large-scale two-dimensional vortices in the side layers, turbulent heat transport is expected to improve the heat removal from the wall. The question of whether this turbulence retains three-dimensional isotropic features or exhibits a more or less strong tendency to a non-isotropic quasi-two-dimensional character is very important with regard to additional pressure losses caused by dissipation of turbulent kinetic energy. Isotropic turbulence in MHD flows is in general extremely dissipative. Its occurrence will cause high additional pressure losses that might annihilate the positive effect of heat transfer improvement by turbulent flow. However, non-isotropy is achieved by the formation of turbulent eddies aligned with the magnetic field, thereby the dissipation of turbulent kinetic energy by Joule's dissipation is significantly reduced and Q2D turbulent flow may be maintained without additional pressure losses.

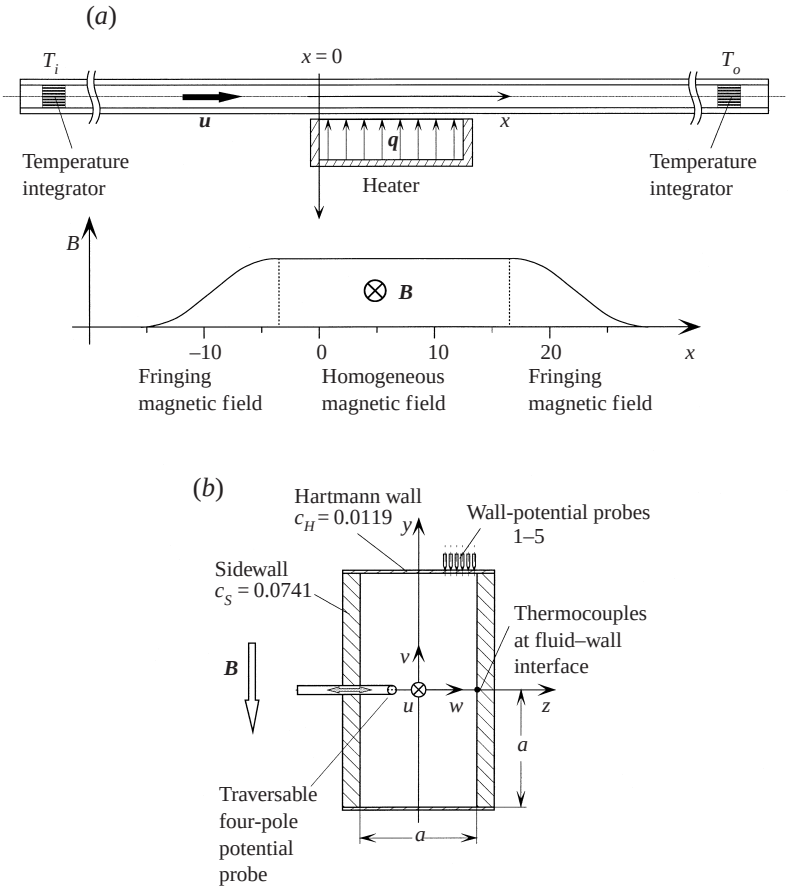

FIGURE 3. Experimental setup. (*a*) Arrangement of the test section and the heater in the magnetic gap and distribution of magnetic induction along the flow direction. (*b*) Cross-section with instrumentation.

4. Experimental setup and instrumentation

The test channel is a rectangular stainless steel tube with an aspect ratio 2 : 1 and a characteristic length of $a = 40\,\text{mm}$. Both sidewalls are 6 mm thick, the Hartmann walls only 1 mm to reduce the Hartmann braking of turbulence. A eutectic sodium–potassium alloy $Na^{22}K^{78}$ is circulated at mean velocities up to $2\,\text{m}\,\text{s}^{-1}$. The wall conductance ratios of the side and the Hartmann walls are calculated from (1.1) as $c_S = 0.0714$ and $c_H = 0.0119$. The heat flux of $q = 15\,\text{W}\,\text{cm}^{-2}$ is produced by an electrically powered radiation heater along a heated length of 500 mm or $12.5a$ respectively. The test section is placed in the gap of an electro-magnet where the intensity of the uniform magnetic field can be varied from 0.25 T up to 2 T. In figure 3(*a*) the arrangement of the test section and the heater in the magnetic gap is sketched.The length scale in this picture is the characteristic length scale of the duct *a*. The graph B versus x illustrates the distribution of the strength of the magnetic field along the axial flow direction. The heater is located in the centre part of the magnetic gap and the beginning of the heated length is defined as $x = 0$. Thus an axial developing length of approximately $11a$ in the fringing field and of $3.75a$ in the region of homogeneous magnetic field is provided before the heated section starts.

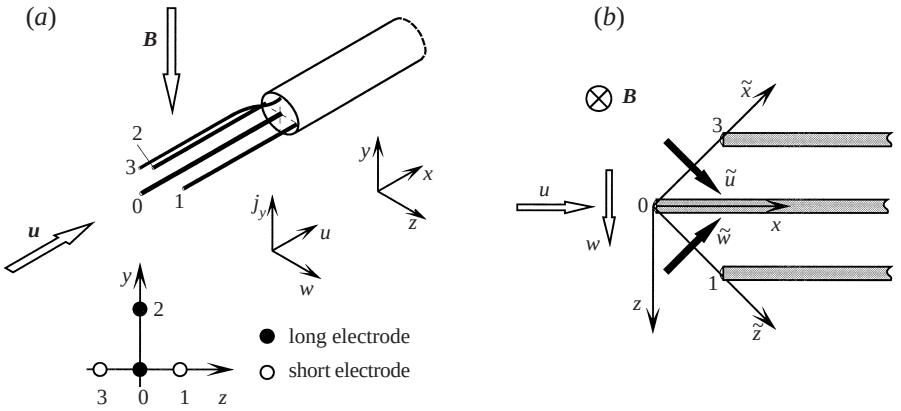

FIGURE 4. (*a*) Geometry and coordinates of the sensing tip of the four-pole temperature-potential probe. (*b*) Evaluation of velocity components u and w.

In figure 3(*b*) a cross-section of the duct is shown including instrumentation. The instrumentation used in this experiment consists of two sets. The first one records the integral quantities like pressure drop and temperatures at the heated wall. Therefore pressure taps with an inner diameter of 2 mm are fitted to the non-heated sidewall at axial distances of $6.25a$ and within the region of homogeneous magnetic field. The average inlet and outlet temperatures T_i and T_o at both ends of the test section are measured by temperature integrators fitted into the duct (see figure 3*a*). In order to measure the temperature at the wall–fluid interface three Cu—CuNi thermocouples with a diameter of 0.5 mm are placed along the centreline ($y = 0$) of the heated sidewall at three different axial positions with a distance of $6.25a$ between each of them.

The second set of instrumentation is installed to record local flow quantities and information about the turbulence structure within the flow. For this purpose probes are traversed in the channel midplane ($y = 0$) in the z-direction. In addition, the electric potential is measured on the outer surface of the Hartmann wall, just above the sensing tip of the probe, by a line of six spring loaded needles. All probe measurements presented here are taken at $x = 12.25$ close to the end of the heated section.

As pressure taps and thermocouples are commonly used and can be considered as well understood instrumentations, we will focus our attention on the use of potential probes. Our measurements are performed with the aid of a four-pole temperature-potential probe, which simultaneously records the potential differences for all three components of $\nabla\phi = (\phi_x, \phi_y, \phi_z)$. This is possible by the non-coplanar arrangement of the four electrodes sketched in figure 4(*a*).Three electrodes $(0, 1, 3)$ are arranged in a plane perpendicular to the magnetic field, a fourth one (2) is placed just above the central one (0) in the direction of the magnetic field. The distance from the tip of the central electrode to the tips of all the other ones is $d_e = 1.41$ mm. This gives a maximal scale of the sensing tip of about 2 mm and a spacial resolution of about $0.1a$. The derivatives of the electric potential are determined by measuring the voltage $\Delta\phi$ between two electrodes distance d_e apart.

In inductionless MHD flows ($Rm \ll 1$), information about the velocity field can be evaluated from the electric potential induced by the fluid motion using Ohm's law (2.4). This technique is known as induction velocimetry and an overview of the principle and the various applications has been given by Shercliff (1962) and Baker

(1983). However, the spanwise and the streamwise velocity components in the plane perpendicular to the magnetic field u and w cannot be calculated until the current density $\boldsymbol{j}$ is known. Reed *et al.* (1986) find that for laminar MHD duct flow the current density in the fluid can be neglected if the condition $1/M \ll c \ll 1$ holds. Sommeria & Moreau (1982) assess the errors caused by neglecting the current density in Q2D flows with insulating walls to be of the order N^{-1}. Although these arguments have often been used, direct information can be obtained from experimental data. Namely, if the magnetic field direction is parallel to the y-direction as in the experiment, the current density $j_y = -\phi_y$ can be evaluated directly (see Kit 1970). The finding of small j_y compared to ϕ_x and ϕ_z, together with the conservation of charge (2.3), may serve as an indication but not proof, that the current density in the plane perpendicular to the magnetic field is also small and the velocities perpendicular to the magnetic field can be evaluated as $u = -\phi_z$ and $w = \phi_x$. This is consistent with the well known tendency of magnetic field to remove gradients along its direction. It is noteworthy that there is an additional mechanism of quasi-two-dimensionalization of the flow structure in the wall-jet region. This is because in this region $\partial/\partial x \sim \partial/\partial z \sim O(1)$, whereas $\partial/\partial y \sim O(M^{-1/2})$. Both effects contribute to the tendency of the local flow structure to become quasi-two-dimensional and both are weakened as the flow in the sidewall jet becomes turbulent. We are not able in this study to distinguish between the two mechanisms.

Figure 4(b) illustrates the determination of the velocity components u and w perpendicular to the magnetic field from the probe measurements. The tips of the electrodes define the $\tilde{x}, \tilde{y}, \tilde{z}$-coordinate system in which the velocity components $\tilde{u}$ and $\tilde{w}$ are determined from Ohm's law (2.4). Transformation onto the x, y, z-coordinate system of the duct yields the velocity components u and w.

In order to measure both the velocity and the temperature simultaneously each electrode is made of a Ni − CrNi thermocouple with a diameter of 0.25 mm. The thermopairing is electrically insulated from the stainless steel jacket measuring the electric potential and therefore cross-talking between the electric potential and temperature measurement is avoided. From such a probe mean values and fluctuations of velocities and temperature can be evaluated and from these the turbulent transport properties of the Reynolds stress tensor and the Reynolds heat fluxes, namely $\overline{u'^2}$, $\overline{w'^2}$, $\overline{u'w'}$, $\overline{u'T'}$ and $\overline{w'T'}$, can be derived.

Moreover, from knowledge of the full gradient vector of the electric potential the degree of isotropy of a turbulent flow can be estimated by several means. Tsinober, Kit & Teitel (1987) derived precise relations between statistical properties of the turbulent velocity and the electric potential field induced by the fluid motion. From their results the following two isotropy coefficients can be defined as a measure for the anisotropy of the turbulent flow:

$$A_x = \frac{2\overline{(\phi'_y)^2}}{\overline{(\phi'_x)^2}}, \qquad A_z = \frac{2\overline{(\phi'_y)^2}}{\overline{(\phi'_z)^2}}. \tag{4.1}$$

In isotropic turbulence both isotropy coefficients A_x and A_z take a value of 1. In perfect two-dimensional turbulence, the absence of any potential difference along magnetic field lines makes the mean square value $\overline{(\phi'_y)^2}$ vanish and both coefficients become zero. A similar behaviour can be expected in Q2D turbulence because the current density in the direction of magnetic field remains small.

The degree of isotropy of fluctuations of a distinct frequency or a frequency range is obtained by evaluating A_x and A_z in terms of coefficients $E_i(f)$ of the one-dimensional

			$Re =$	3.3×10^3	1.5×10^4	3.0×10^4	6.0×10^4	1.0×10^5
			$u_0\,(\mathrm{m\,s^{-1}}) =$	0.08	0.32	0.64	1.28	2.00
$M =$	600	B (T) = 0.25	$N =$	109	24	12	6	3.6
	1200	0.5		436	96	48	24	14.4
	2400	1.0		1745	384	192	96	57.6
	3300	1.4		6982	1536	768	384	230
	4800	2.0		27927	6144	3072	1536	922

TABLE 1. Non-dimensional parameters Re, M, and $N = M^2/Re$ and approximate dimensional values of mean velocity u_0 and magnetic field B.

power spectra of $\nabla\phi$:

$$A_x(f) = \frac{2E_y}{E_x}, \qquad A_z(f) = \frac{2E_y}{E_z}. \tag{4.2}$$

A further important assessment of the degree of isotropy can be obtained from the probability density function (PDF)

$$P_{\cos\theta} = \mathrm{PDF}\,(\cos\,[\boldsymbol{B}, \nabla\phi']) \tag{4.3}$$

of the cosine of the angle $\theta \doteqdot [\boldsymbol{B}, \nabla\phi']$ between the direction of the magnetic field $\boldsymbol{B}$ and the fluctuating part of $\nabla\phi$. Figure 5 shows the following principal behaviour of the PDF: In purely two-dimensional turbulent flow, the fluctuating part of $\nabla\phi$ is strictly perpendicular to the magnetic field and thus $\cos\theta$ is always zero. In this case the PDF is a delta function. Deviations from the pure two-dimensional state are indicated as the PDF broadens. In the limiting case of isotropic turbulence all angles θ occur with the same probability and the PDF of θ becomes a white noise distribution.

For Q2D flow, variations of the electric potential across the Hartmann layers are expected to be negligible and therefore the distribution of the electric potential of the core region is expected to be mapped onto the Hartmann walls. Therefore, similarly to the evaluation of the probe signals, the electric potential difference, measured between two electrodes at the Hartmann wall, can be used to evaluate the axial velocity by the relation $u_w = -\phi_z$.

5. Results for isothermal flow

For investigating the characteristics of isothermal flow a first series of experiments has been performed without heating the sidewall. In table 1 the corresponding parameters are summarized. Also, dimensional values of the magnetic field and the velocity are given. If not mentioned otherwise, all results are presented in non-dimensional form according to the scaling introduced in § 2.

5.1. *Laminar velocity distribution and onset of instabilities*

At small flow rates no fluctuations of the electric potential recorded by the probe are observed and the flow is therefore characterized as laminar. In figure 6(*a*) the distribution of the axial velocity component u in the midplane ($y = 0$) is plotted in one half of the cross-section for $Re = 3.3 \times 10^3$ and Hartmann numbers 600, 1200, 2400 and 4800. The known tendencies of increasing peak velocity coupled with decreasing thickness of the side layer at increasing Hartmann number is well represented by the

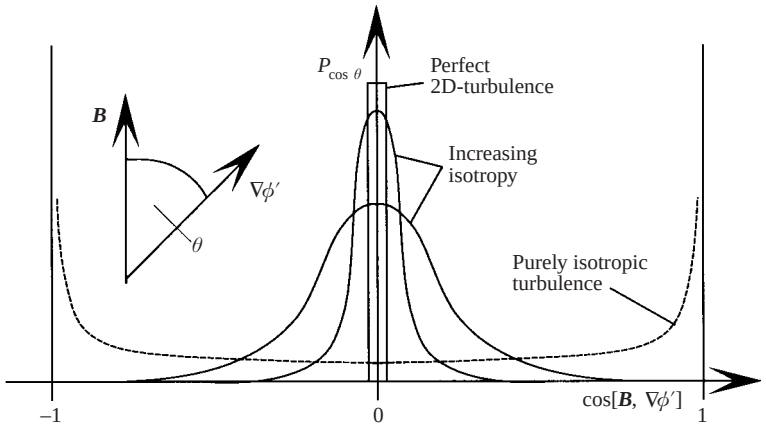

FIGURE 5. Propabillity density functions $P_{\cos\theta}$ of the angle between the magnetic field $\boldsymbol{B}$ and the fluctuating part of the gradient of the electric potental $\nabla\phi'$.

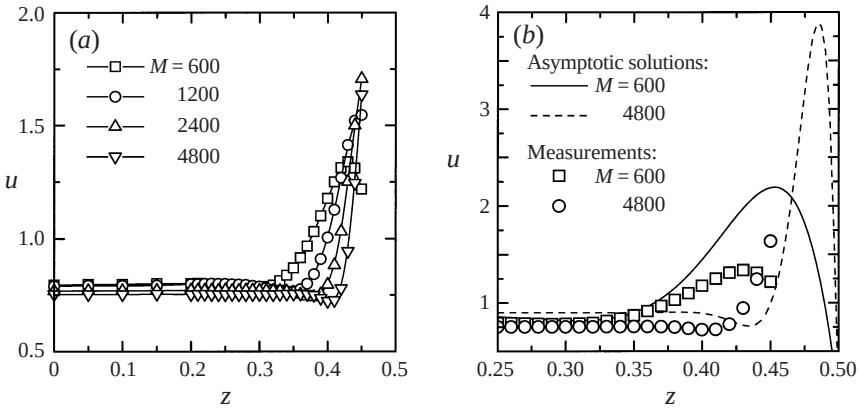

FIGURE 6. (*a*) Measured laminar velocity distributions in the midplane ($y = 0$) for various Hartmann numbers. (*b*) Comparison of measured velocity distributions at $M = 600$ and $M = 4800$ (symbols) with results of an asymptotic solution (lines). The measured results are obtained for $Re = 3.3 \times 10^3$.

measurements. Because of insufficient resolution of the probe the velocity could not be evaluated closer to the wall than up to the position $z = 0.45$. In figure 6(*b*) the measured velocity distributions at $M = 600$ and $M = 4800$ are compared with results from an asymptotic solution in the jet region. The asymptotic solution overestimates the peak velocity in the jet as clearly seen at $M = 600$, whereas the width of the jet is clearly underestimated. However, the measured and the calculated velocities in the core region agree very well. Whether the deviations in the side layer arise from an interaction of the probe with the jet or whether it is a real flow effect cannot be clarified by other means in this experiment.

As the Reynolds number is increased beyond a critical value Re_c, fluctuations of the probe signals associated with local unsteady flow phenomena are observed in the side layers, in the range $0.40 < z < 0.45$. In figure 7 the influence of different Hartmann numbers on the experimentally observed critical Reynolds number Re_c is shown. Within the range of Hartmann numbers investigated the change of the critical Reynolds number is not significant from a technical point of view. However some decrease of the critical Reynolds number with increasing Hartmann numbers at a

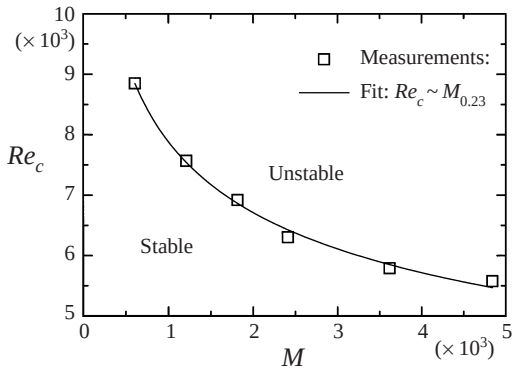

FIGURE 7. Dependence of the critical Reynolds number Re_c for the onset of instabilities in the side layers on the Hartmann number M.

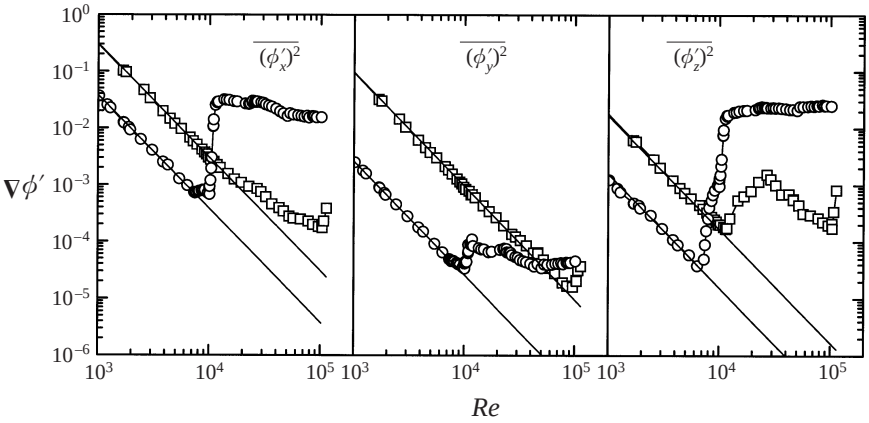

FIGURE 8. Mean-square values of the fluctuating part of the electric potetial gradient $\nabla\phi'$ recorded by the probe at $z = 0.45$. The Reynolds number is increased from laminar to turbulent flow for $M = 600$ (squares) and $M = 4800$ (circles).

rate close to $M^{-1/4}$ is observed from the measurements. This observation supports the conjecture of stronger nonlinearities at higher Hartmann numbers made in § 3 and is in contradiction with the results of a linear stability analysis performed by Ting *et al.* (1991). They predict the critical Reynolds number to be independent of the Hartmann number. But it has to be mentioned that the measurement of the critical Reynolds number may also be influenced by the decreasing sensivity of the potential probe at lower magnetic fields.

5.2. *The degree of anisotropy*

In order to evaluate velocity fluctuations from the electric potential probe (see figure 4) the fluctuations of the electric potential in the direction of the magnetic field have to be small compared to those in directions perpendicular to the magnetic field. This matter is discussed in terms of the mean values $\overline{(\phi'_x)^2}$, $\overline{(\phi'_y)^2}$ and $\overline{(\phi'_z)^2}$ of all components of the electric potential gradient $\nabla\phi$, evaluated from the probe. In figure 8 results obtained in the near-wall position $z = 0.45$ and for the lowest and the highest experimentally realized Hartmann number are plotted versus the Reynolds number.

In the laminar flow region ($Re < 6000$) a formal evaluation of the probe voltage

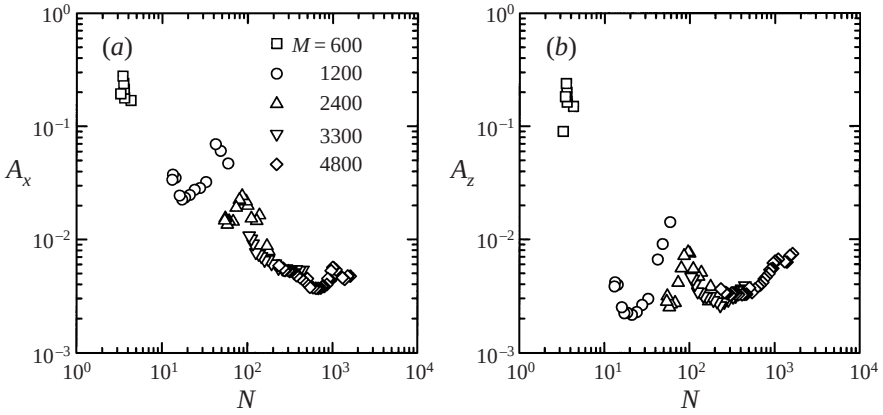

FIGURE 9. Variation of isotropy coefficients at $z = 0.45$ with the interaction parameter of duct flow N: (*a*) A_x in the streamwise and (*b*) A_z in the spanwise direction.

output gives non-zero mean-square values due to random noise of the electronic circuitry. Due to the scaling of the electrical potential with the magnetic field B and the flow rate u_0 (see § 2) the noise level decreases generally with the Reynolds number as Re^{-2}. Since the contribution of noise to the mean-square value is independent of the flow rate, the level of noise determined in the laminar region may be extrapolated to higher Re by a straight line of slope -2. If the Reynolds number exceeds its critical value, the mean-square values emerge from their individual level of noise and a measurable signal caused by turbulent velocity fluctuations is clearly identified in figure 8. In the time-dependent region the mean-square values grow fast, but level off for the high Hartmann number $M = 4800$ to a saturation level and thus become practically independent of the Reynolds number. Similar behaviour can be observed down to a Hartmann number of $M = 1200$. At the lower Hartmann number $M = 600$ all contributions of $\overline{(\nabla\phi')^2}$ are significantly smaller than for $M = 4800$. It may be conjectured that the reduced shear of the sidewall jet here is too weak to promote intense velocity fluctuations. Although $\overline{(\phi'_x)^2}$ and $\overline{(\phi'_z)^2}$ are increasing fast above critical conditions at $M = 600$ they decrease again at high Reynolds numbers. Most probably this effect is related to a not fully developed state of the turbulent flow because the interaction parameter that governs the temporal evolution of the turbulent flow decreases with both decreasing M and increasing Re.

At $M = 600$, $\overline{(\phi'_y)^2}$ emerges from the level of noise only at the very high Reynolds numbers $Re \geqq 10^5$ and no relevant value of $\overline{(\phi'_y)^2}$ is obtained for $Re \leqq 10^5$. From the significantly higher values of $\overline{(\phi'_x)^2}$ and $\overline{(\phi'_z)^2}$ in the turbulent region a strong non-isotropic, quasi-two-dimensional turbulence structure can already be expected at $M = 600$. Formally this is obtained by applying the isotropy relations (4.1) with the assumption of $\overline{(\phi'_y)^2} \approx 0$. In case of the high Hartmann number $M = 4800$ the value of $\overline{(\phi'_y)^2}$ differs significantly from the noise and the conditions (4.1) and (4.2) can be applied quantitatively to judge the degree of anisotropy in the flow.

In figure 9 the isotropy coefficients A_x and A_z are plotted versus the interaction parameter N at the near-wall position $z = 0.45$. The measurements were performed at Hartmann numbers in the range $600 < M < 4800$ and only those values are taken into account where $\overline{(\phi'_y)^2}$ significantly exceeds the level of noise.

With increasing interaction parameter both isotropy coefficients generally decrease.

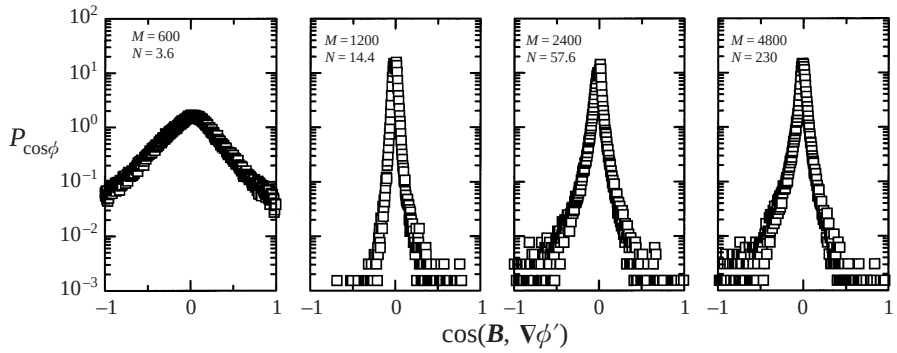

FIGURE 10. The influence of increasing Hartmann numbers at constant Reynolds number $Re = 1.0 \times 10^5$ on the propability density function of the cosine of the angle between applied magnetic field and the fluctuating part of the electric potential gradient $P_{\cos\theta} = \mathrm{PDF}(\cos[\boldsymbol{B}, \nabla\phi'])$. The signals are recorded close to the sidewall at $z = 0.45$.

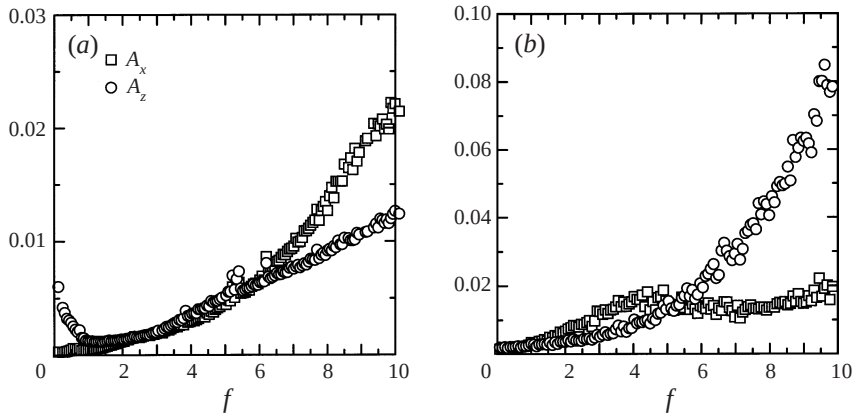

FIGURE 11. Frequency dependence of isotropy coeficients $A_x(f)$ and $A_z(f)$. The signals are recorded at $M = 4800$ close to the sidewall at $z = 0.45$. (*a*) $Re = 3.0 \times 10^4$ and (*b*) $Re = 1.0 \times 10^5$.

This indicates that the turbulent flow becomes less isotropic when N is increased as it is predicted from (3.1). Moreover, the differences between the two coefficients A_x and A_z show that the turbulent velocity fluctuations are not even isotropic in the plane perpendicular to the magnetic field at this position of the probe.

In figure 10 the isotropy of the velocity field is characterized by the PDF of the cosine of the angle between magnetic field and $\nabla\phi'$ defined by relation (4.3). Here, a series of PDFs for increasing Hartmann numbers at the highest achievable Reynolds number $Re = 1.0 \times 10^5$ is presented.

At the lowest Hartmann number $M = 600$ the non-zero values of the $P_{\cos\theta}$ function have a maximum around $\cos[\boldsymbol{B}, \nabla\phi'] = 0$ and anisotropy of the turbulent flow is thus clearly indicated. The increase of the Hartmann number to $M = 1200$ results in a spiky shape of the $P_{\cos\theta}$ function that indicates a much higher degree of anisotropy of turbulence. If the Hartmann number is further increased to $M = 2400$ and $M = 4800$, the $P_{\cos\theta}$ functions broaden again showing a clear tendency of the turbulent flow to more isotropy. This effect is presumably due to the increased shear in the side layers at higher magnetic fields that leads to stronger nonlinearity. The interaction parameter of $N = 3.6$ ($M = 600$ and $Re = 1.0 \times 10^5$) is the smallest that can be achieved in the

test facility employed. An increase in Hartmann number or a decrease of Reynolds number result in higher interaction parameters and thus increase the tendency towards two-dimensionality. This fact has been validated by the similar behaviour of the $P_{\cos\theta}$ function observed for measurements performed at other parameters.

From the non-dimensional decay time of isotropic turbulence given by expression (3.1) a tendency to higher isotropy is expected also for the smaller turbulence scales. In figure 11 the isotropy coefficients A_x and A_z obtained from power spectra (see equation (4.2)) are plotted versus the frequency f for a Hartmann number of $M = 4800$ and the two Reynolds numbers $Re = 3.0 \times 10^4$ and $Re = 1.0 \times 10^5$ respectively. The frequency f is normalized with the advection time of the duct flow. Using Taylor's hypothesis, meaning that vortices are convected with the mean velocity, one can obtain an appropriate non-dimensional length scale for the vortex dimension. At both Reynolds numbers the spectral values of the isotropy coefficients are increasing with increasing frequency. This observation supports our conjecture that a higher degree of isotropy can generally be observed at smaller length scales. Moreover a comparison of both diagrams shows that the tendency to higher isotropy at smaller scales is more significant at smaller interaction parameter. Although the isotropy coefficients become larger for small-scale turbulent structures, i.e. for higher frequencies, even the smallest vortices detectable by the probe and corresponding to $f \approx 10$ remain strongly non-isotropic.

From the evaluation of the isotropy coefficients and the corresponding PDFs it can be inferred that the turbulence in the side layer has at least locally a non-isotropic, two-dimensional structure in the whole range of parameters investigated. In such a turbulent MHD flow the current density in the fluid remains small in the sense that the fluctuations of the potential gradient in the direction of the magnetic field are small compared to those in the directions perpendicular to the magnetic field. As outlined in § 4 the time-dependent transverse velocities u and w can now be evaluated from the electric potential using Ohm's law.

5.3. *The structure of the turbulent flow*

The structure of Q2D turbulent MHD flow is significantly different from ordinary turbulent flows. Instead of a three-dimensional cascading process towards smaller scales, Q2D vortices tend to evolve into larger structures forming more regular flow patterns than ordinary turbulence.

Careful observations of the flow in the range of parameters have shown a variety of time-dependent flow phenomena. Here we will focus the discussion on dominant effects and certain similarities observed in broad parameter ranges.

An impression of the structure of the turbulent flow in the side layer can be obtained from the time series of the signals of the probe at the position $z = 0.45$ and of all wall potential-difference probes (see figure 3*b*). The fluctuating parts of these signals are plotted all together in figure 12 for the Hartmann number $M = 4800$ and the Reynolds number $Re = 1.5 \times 10^4$.

Significant fluctuations of the velocity components u' and w' with an amplitude comparable with the mean flow velocity are visible from the time series of the probe. These fluctuations can be associated with large vortices which either occur in regular groups or as single events. Small-scale structures with different durations occur between the vortex groups or even individual vortices. The current density component in the direction of magnetic field j'_y shows no significant fluctuations and thus underlines again that the turbulent flow is Q2D even in the small scales.

The streamwise velocity fluctuations $u'_{w,5}$ recorded on the Hartmann wall in the

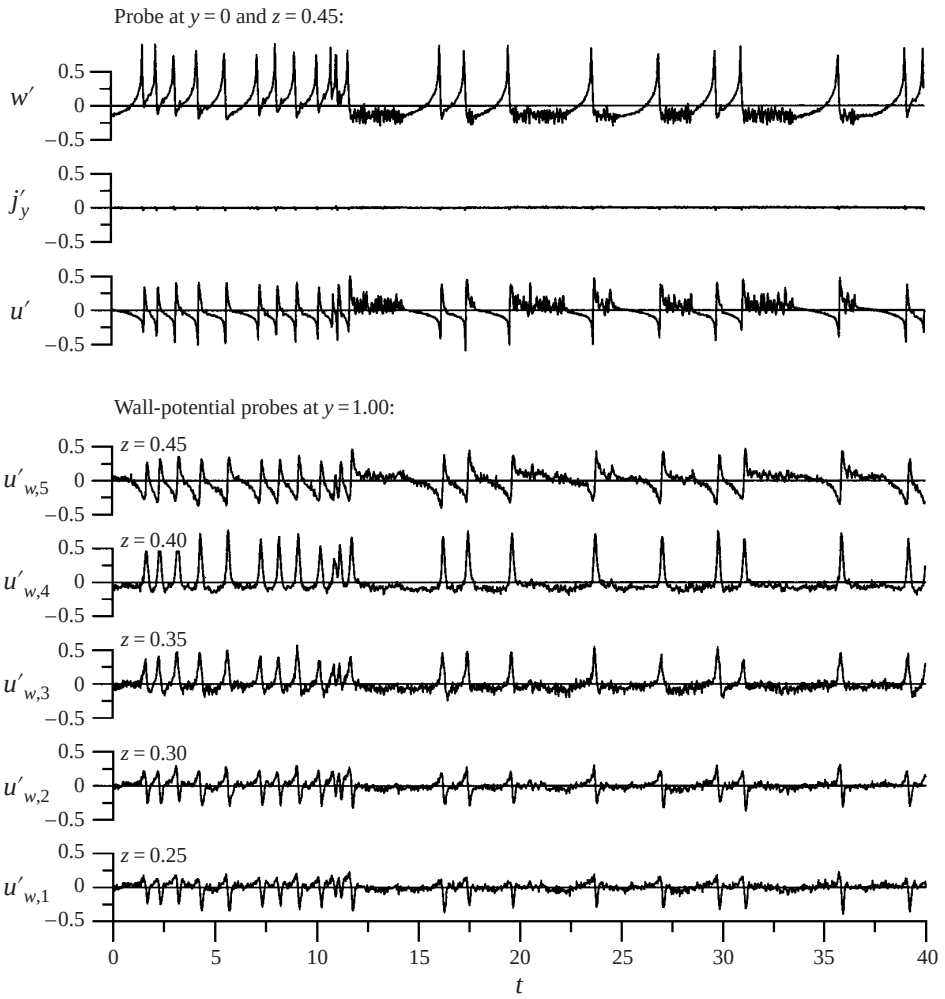

FIGURE 12. Time series of the fluctuating parts of the probe signals at $z = 0.45$ and the potential probes on the Hartmann wall for $M = 4800$ and $Re = 1.5 \times 10^4$.

same position $z = 0.45$ as the probe are very well correlated with the signals of the probe u'. On the other hand the amplitude of the signal is about a factor of 10 smaller. Although the eddies identified in the midplane are clearly aligned with the magnetic field up to the Hartmann walls, their fluctuating intensity is detected as being much smaller by measurements on the Hartmann wall and the strong non-isotropy detected by the probe is therefore valid locally only. It cannot be explained clearly from the instrumentation installed in this test section whether the intensity of vortices decreases continuously from the midplane to the Hartmann walls or whether it is only limited to the Hartmann layers. However, velocity fluctuations measured at the Hartmann wall give at least a qualitative picture of the turbulent flow in the core region of the duct. Comparing the time series recorded by all the wall potential probes, we find that the amplitudes of the large vortices are detected simultaneously along the whole chain of installed wall probes. The signals can be interpreted as turbulent flow characterized by large eddies of approximately uniform size which are convected downstream at a constant distance from the sidewall as sketched in figure 1.

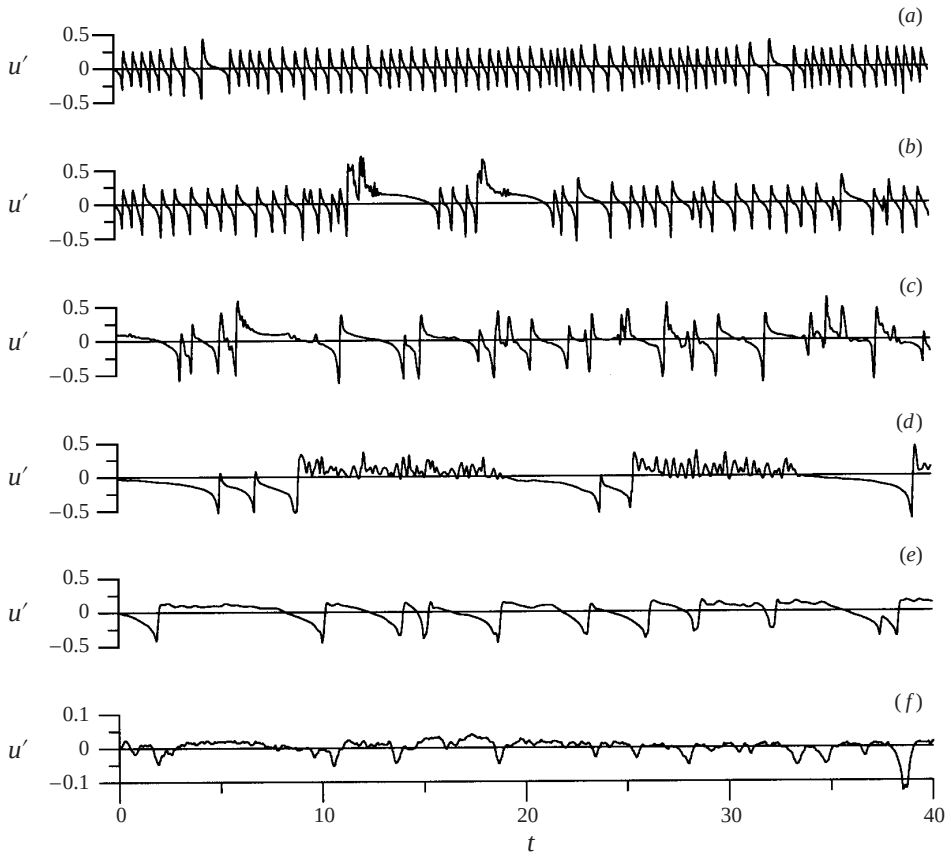

FIGURE 13. Time series of the fluctuating part of the streamwise velocity u' at $z = 0.45$. The change in turbulence structure: due to increasing Reynolds number (*a*) $Re = 3.0 \times 10^4$, (*b*) $Re = 6.0 \times 10^4$ and (*c*) $Re = 1.0 \times 10^5$ at constant Hartmann number $M = 4800$; due to decreasing Hartmann number (*c*) $M = 4800$, (*d*) $M = 2400$, (*e*) $M = 1200$ and (*f*) $M = 600$ at constant Reynolds number $Re = 1.0 \times 10^5$.

Starting with this turbulent flow at high Hartmann number and moderate Reynolds number we shall next study the effects of first increasing the Reynolds number and then reducing at constant Reynolds number the Hartmann number. In figure 13(*a–f*) the change in turbulence structure is illustrated by the fluctuations u' of the streamwise velocity only.

The intermittent behaviour of the signal at $M = 4800$ and $Re = 1.5 \times 10^4$ in figure 12 changes at $Re = 3.0 \times 10^4$ (figure 13*a*) to a quasi-periodic pattern representing regular events from the passing of large vortices. By further increasing the Reynolds number this high degree of order is lost. At $Re = 6.0 \times 10^4$ the periodic pattern is replaced by sudden large-amplitude excursions followed by quiet periods. Isolated large fluctuations dominate the flow at $Re = 1.0 \times 10^5$ and the flow may be considered as an intermittently turbulent state containing vortices of different size and intensity.

The decrease of Hartmann number from $M = 4800$ (figure 13*c*) to $M = 2400$ (figure 13*d*) at constant Reynolds number $Re = 1.0 \times 10^5$ results in long periods of quasi-regular oscillations with less-organized small-scale fluctuations in between. Large fluctuations occur rarely. If the Hartmann number is further reduced to $M = 1200$ (figure 13*e*) a more regular signal pattern emerges again. At $M = 600$

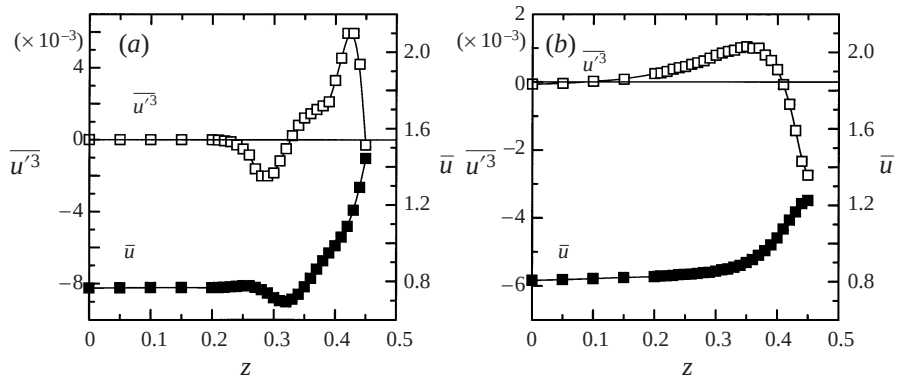

FIGURE 14. Third-order moment $\overline{u'^3}$ and streamwise mean velocity $\bar{u}$ in the midplane $y = 0$. Two different distributions of $\overline{u'^3}$ with respect to $\bar{u}$ result in two different shear layer instabilities. (*a*) *Type I Instability* at $M = 4800$, $Re = 3.0 \times 10^4$ and (*b*) *Type II Instability* at $M = 1200$, $Re = 1.0 \times 10^5$.

(figure 13*f*) the turbulence intensity in terms of signal fluctuations gets significantly weaker, but more irregular.

All recordings of u' at the high Hartmann number $M = 4800$ are approximately symmetric with regard to the zero value and the related vortices are interpreted to occur in a more or less regular column at the wall side of the jet as demonstrated in figure 13(*a–c*). At lower Hartmann numbers (figure 13*d–f*) the large fluctuation amplitudes recorded in the near-wall position of the probe are for the most part negative and thus the large fluctuations occur mainly against the main direction of flow. This observation can also be investigated qualitatively by evaluating the third-order moments of the streamwise velocity $\overline{u'^3}$ and comparing their distribution along the z-axis with the mean velocity $\bar{u}$ as it is done in figure 14.

At $M = 4800$ and $Re = 3.0 \times 10^4$ (figure 14*a*) an anticlockwise direction of rotation of the periodic vortex pattern is clearly demonstrated from the distribution of $\overline{u'^3}$. We call this type of flow with downstream fluctuations close to the sidewall *Type I Instability*. From the mean velocity distribution the centre of rotation (indicated by a change in sign of $\overline{u'^3}$) of all vortices is obviously located in the outer, bulk-side shear layer of the sidewall jet. The source of energy supply to these vortices therefore originates from the jet shear layer facing the channel bulk flow (outer shear layer).

In figure 14(*b*) an opposite sense of rotation, namely clockwise rotation, is indicated for $M = 1200$ and $Re = 1.0 \times 10^5$. This observation is interpreted as an instability of the wall-side shear layer (inner shear layer) at the side of the jet adjacent to the wall and is called *Type II Instability*. The vortices of this instability are generated in the inner shear layer and are turning clockwise. However their centre of rotation, indicated by the change in sign of $\overline{u'^3}$ lies on the inner side of the jet. This phenomenon cannot be explained by the picture of a vortex column along the sidewall generated and maintained by the shear of the sidewall jet. The time recordings of u' in figure 13(*b*) at this set of parameters indicate large fluctuations between long time periods with upstream flow. These large vortices cause a breakdown of the jet structure in their vicinity and a monotonic decrease of the core velocity to the sidewalls is obtained as in OHD flows. Thus the direction of shear is in agreement with the clockwise rotation of vortices. Between the isolated vortices the jet structure is maintained and we observe by averaging over a long time period a mean velocity distribution with sidewall jets. As the probe does not resolve the region $z > 0.45$ no information on the flow structure of the wall-side shear layer is obtained from the present experiment.

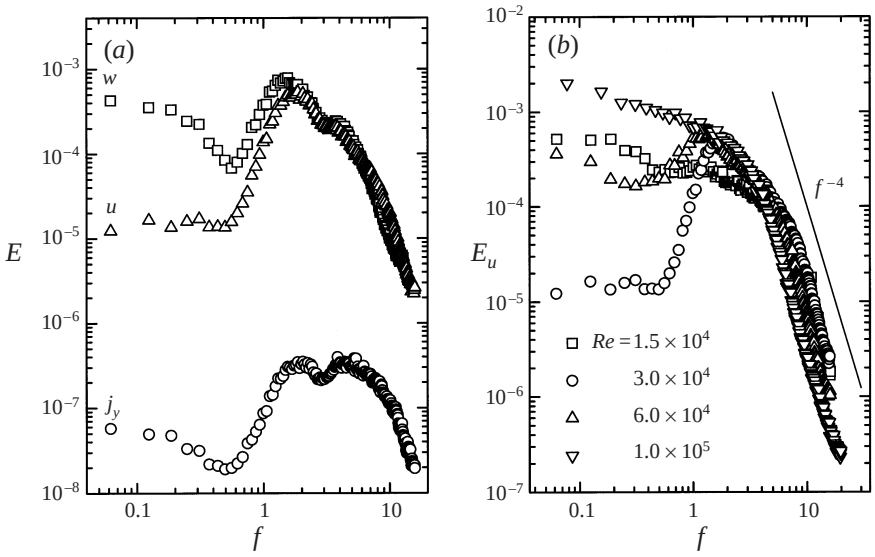

FIGURE 15. (*a*) Power spectra E of the velocities u, v and the current density j_y measured by the probe for $M = 4800$ and $Re = 3.0 \times 10^4$. (*b*) The influence of increasing Reynolds number on the power spectra E_u of the streamwise velocity u for $M = 4800$. All measurements are taken at $z = 0.45$.

In figure 15(*a*) power spectra of all signals (u, j_y, w) recorded at the position $z = 0.45$ at the highest Hartmann number $M = 4800$ and the Reynolds number $Re = 3.0 \times 10^4$ are plotted versus frequency.

All power spectra show a distinct peak which can be identified with the distance between large vortices and their transport velocity at these parameters. Beyond this peak the power decays steeply until the spatial resolution of the probe at $f \approx 10$ is reached. The power spectrum of the current density component in the direction of magnetic field behaves in a similar way as those of the velocity components. But if we calculate the frequency dependence of isotropy coefficients as was done in figure 11(*a*) from the same data, it becomes obvious that the higher isotropy of turbulence in the high-frequency range is reflected in the energy spectra by a less steep decrease of the current density component in the direction of magnetic field.

Since the characteristics of the spectral distribution of turbulent kinetic energy is well represented by one velocity component, the power spectra are further discussed only with the help of the streamwise velocity u. In figure 15(*b*) the effect of increasing the Reynolds number at constant Hartmann number $M = 4800$ is shown. With regard to the quasi-periodic signal at $Re = 3.0 \times 10^4$ in figure 13(*a*) the less regular and more intermittent states are reflected in the disappearance of the pronounced peak in the spectra and, moreover, by the higher spectral power in the low-frequency range at both higher and lower Reynolds number. In the high-frequency range all the power spectra decay as f^{-4} which seems to be universal for such strongly non-homogeneous anisotropic turbulence. The evaluation of power spectra for lower Hartmann numbers has shown that generally the intensity of the fluctuations decreases for lower magnetic fields; besides that fact the power spectra are similar.

We conclude that the turbulent flow in the side layers consists mostly of large scale structures of $l_\perp > 0.1a$; smaller scales reaching down to the limit of spatial resolution of the probe used do not contribute significantly to the integral flow quantities such

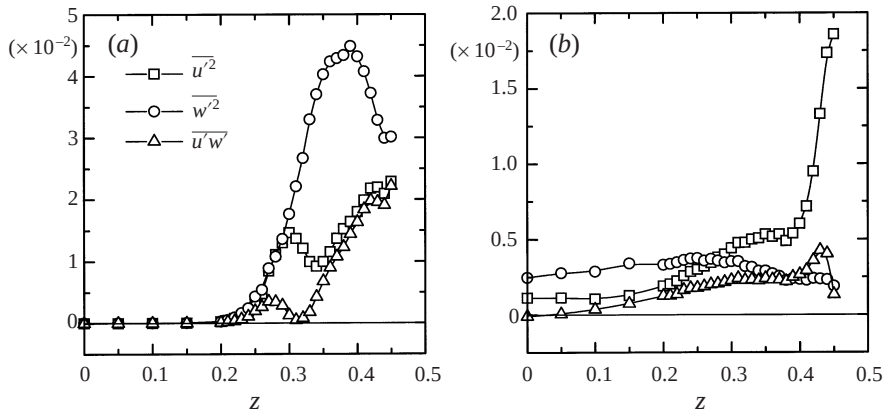

FIGURE 16. Distribution of Reynolds stresses in the midplane ($y = 0$) along the z-direction for two characteristic sets of parameters. (*a*) *Type I Instability* at $M = 4800$, $Re = 3.0 \times 10^4$ and (*b*) *Type II Instability* at $M = 1200$, $Re = 1.0 \times 10^5$.

as the turbulent kinetic energy or the Reynolds stresses discussed in the following section.

5.4. *Turbulent Reynolds stresses*

In order to develop MHD turbulence models the distributions of time-averaged flow quantities and the Reynolds stresses have to be known. The latter reduce in Q2D flows to $\overline{u'^2}$, $\overline{w'^2}$ and $\overline{u'w'}$.

In figure 16 the distribution of the Reynolds stresses $\overline{u'^2}$, $\overline{w'^2}$ and $\overline{u'w'}$ are plotted along the channel centreline between the Hartmann walls for the same set of parameters as given in figure 14.

For the quasi-periodic signal of *Type I Instability* at $M = 4800$ and $Re = 3.0 \times 10^4$ the Reynolds stresses are confined to the sidewall regions. In the core no turbulent transport of momentum is observed. The normal stress in the streamwise direction $\overline{u'^2}$ shows two maxima that can be attributed to one-sided fluctuations in the down- and upstream direction respectively caused by the bypassing vortices (see figure 1). The different peak values reflect the deformation of the vortices by the shear in the jet. Corresponding to this interpretation the normal stress in the spanwise direction $\overline{w'^2}$ has only one broad peak caused by the momentum exchange between the regions of large $\overline{u'^2}$. In fully developed turbulent flow the tangential stress $\overline{u'w'}$ is the only contribution of the Reynolds stress tensor that affects the mean velocity distribution. In the region of one-sided downstream fluctuations $\overline{u'w'}$ increases and indicates momentum transport towards the core region. Momentum is transported out of the region of one-sided upstream fluctuations towards the core as well as back into the side layer. The decrease of the Reynolds stress to zero at the sidewall cannot be detected by the probe because of the limited spatial resolution.

As the normal stresses are always positive definite the reverse rotation of *Type II Instability*, discussed in § 5.3, figure 14(*b*), of the vortices for $M = 1200$ and $Re = 1.0 \times 10^5$ cannot be identified in figure 16(*b*). The large values of $\overline{u'^2}$ close to the sidewall represent the zone of one-sided upstream fluctuations in the boundary layer; the region of one-sided downstream fluctuations extends over a wider range. The normal stress in the transverse direction is almost evenly distributed along the cross-section. The continuous decrease of $\overline{u'w'}$ from the side layer towards the core indicates

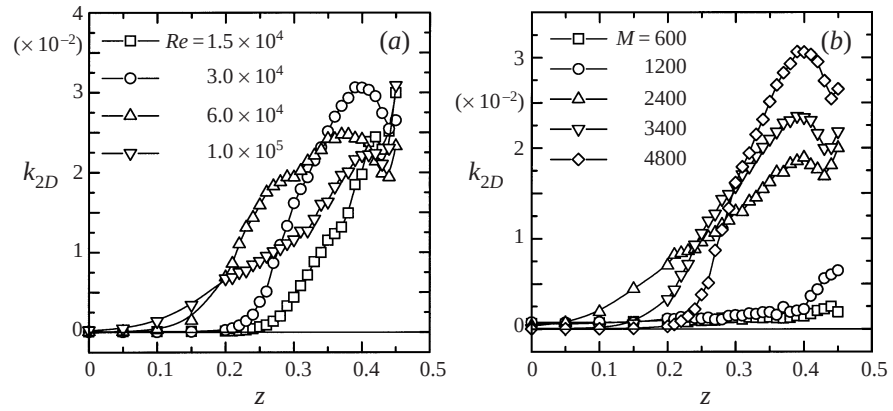

FIGURE 17. Turbulent kinetic energy of two-dimensional turbulence $k_{2D} = (\frac{1}{2})(\overline{u'^2} + \overline{w'^2})$ in the midplane ($y = 0$). (*a*) The effect of increasing Reynolds number at $M = 4800$. (*b*) The effect of different Hartmann numbers at $Re = 1.0 \times 10^5$.

that turbulent transport of momentum from the side layer region acts against the streamwise pressure gradient in the whole core region.

From the non-vanishing normal stress in the core region it is obvious that turbulence penetrates the whole cross-section. As the third-order moment in figure 14(*b*) indicates no preferred direction of rotation in the core region, the turbulent motions there can be considered as a relic of vortices that entered from both side layers into the core region where they dissipate without being further forced by shear.

In perfect two-dimensional as well as in Q2D turbulent flows the turbulent kinetic energy is defined by two velocity components only, i.e. $k_{2D} = (\frac{1}{2})(\overline{u'^2} + \overline{w'^2})$. In order to quantify the turbulence intensity in different flow regions its distribution along z is plotted in figure 17.

At constant high Hartmann number $M = 4800$ (figure 17*a*) the turbulent kinetic energy in the sidewall region reaches comparable values of about $k_{2D} = 0.025$ although the Reynolds number is varied within considerable range $1.5 \times 10^4 < Re < 1.0 \times 10^5$. When the Hartmann number is increased from $M = 600$ up to $M = 4800$ at constant Reynolds number $Re = 3.0 \times 10^4$ (see figure 17*b*), a continuous increase of turbulent kinetic energy in the side layers is observed and the turbulence promoting effect of the magnetic field is well illustrated.

Although a considerable decrease of turbulent kinetic energy from the side layer to the core region is observed in all measurements, the flow close to the centreplane remains weakly turbulent for some parameters investigated, e.g. $Re = 3.0 \times 10^4$ and $M = 1200$. In figure 18 the turbulent kinetic energy in the symmetry plane $z = 0$ is plotted versus the dimensionless decay time of Q2D flow given by relation (3.3) assuming for all parameters the same transverse length scale of the vortices $l_\perp = 0.4$.

A clear increase of the turbulent kinetic energy in the centreplane is observed for increasing decay time. This finding is consistent with the conjecture that turbulent Q2D eddies being released from the turbulent side layers can penetrate the core region before their kinetic energy is removed by Hartmann braking.

Although there is some weak turbulence in the core region at high Reynolds numbers and low Hartmann numbers, a laminar core flow is clearly observed for high Hartmann numbers and for moderate Reynolds numbers as shown in figure 16(*a*) and an evaluation of the width δ of the turbulent side layers becomes possible.

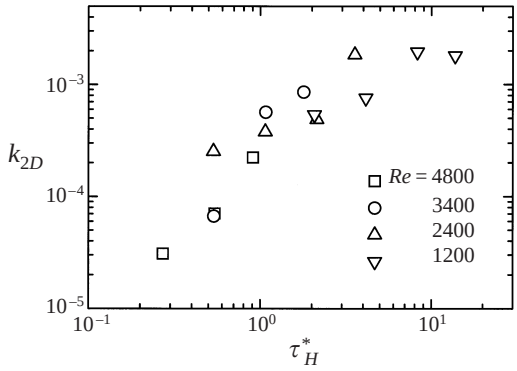

FIGURE 18. Turbulent kinetic energy in the centre of the duct $z = 0$ versus the non-dimensional decay time of Hartmann braking τ^*_H calculated from equation (3.3) with $l_\perp = 0.4$.

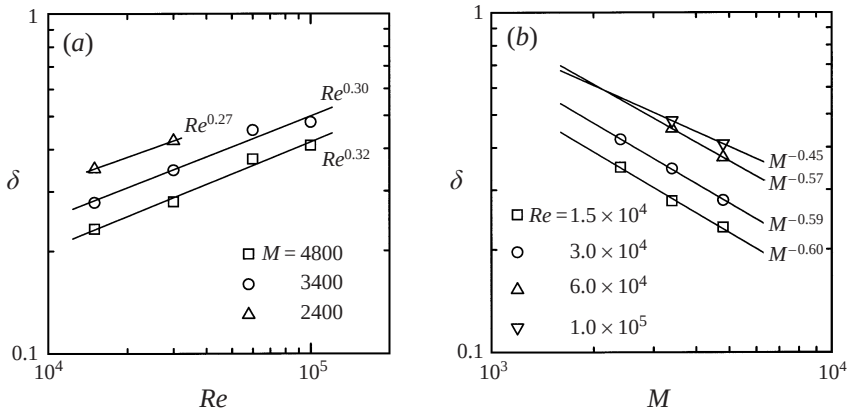

FIGURE 19. Width of the turbulent side layer δ defined as the distance betwen the point where k_{2D} exceeds a value of $k_{2D} = 10^{-3}$ and the sidewall. (*a*) The increase with Reynolds number at constant Hartmann numbers. (*b*) The decrease with Hartmann number at constant Reynolds numbers.

In order to obtain a clear definition, δ is defined as the distance between the point where the turbulent kinetic energy exceeds a threshold value of $k_{2D} = 1 \times 10^{-3}$ and the sidewall.

In figure 19(*a*) the width of the turbulent side layer at constant Hartmann numbers $M = 4800$, $M = 3400$ and $M = 2400$ is plotted as a function of the Reynolds number.

Linear interpolation of the measured values shows that the width increases at constant Hartmann number as the power $Re^{0.3 \pm 0.02}$. In figure 19(*b*) the width of the turbulent side layer at an overall constant Reynolds number evaluated from the same measurements is plotted as a function of the Hartmann number. Here a functional decrease as the power $M^{-0.53 \pm 0.07}$ is found which is different from the power law $M^{-0.5}$ of the laminar jet except for the highest Reynolds number. Combining both results to give $\delta \sim Re^{0.3 \pm 0.02} M^{-0.53 \pm 0.07}$ and expressing the Reynolds number in terms of M and N, however, one observes that δ becomes almost independent of M and it depends on N as $\delta \sim N^{-0.3 \pm 0.02}$. This result confirms with adequate accuracy the assumption by Reed & Picologlou (1989) that $\delta \sim N^{-1/3}$.

Although important for the transport of passive scalar quantities such as heat, the presence of non-zero turbulent kinetic energy does not necessarily mean that there

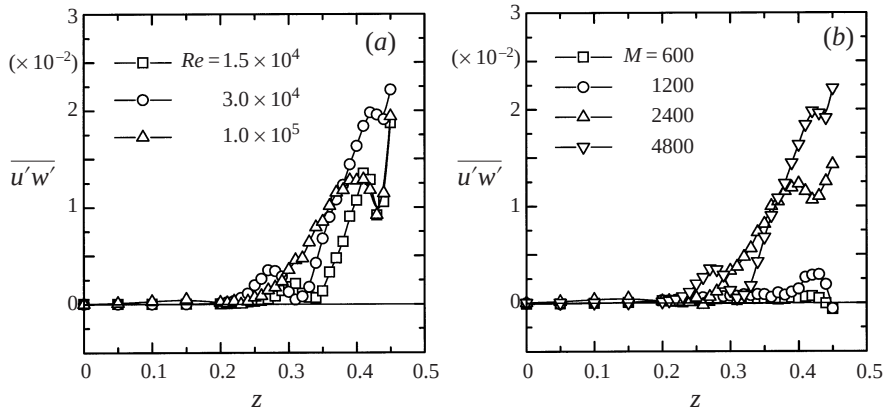

FIGURE 20. Distribution of Reynolds shear stress $\overline{u'w'}$ in the midplane ($y = 0$). (a) The influence of Reynolds number at constant Hartmann number $M = 4800$ and (b) the influence of Hartmann number at constant Reynolds number $Re = 3.0 \times 10^4$.

is turbulent transport in this region. Therefore, the dependence of $\overline{u'w'}$ on the same set of parameters as used for the graph of the turbulent kinetic energy in figure 17 is shown in figure 20.

The magnitude of the Reynolds stresses in the side layer is similar to that of the turbulent kinetic energy and shows the same dependences on Reynolds and Hartmann numbers. Within the range $-0.2 < z < 0.2$ almost no turbulent momentum transport is observed unless turbulent kinetic energy is not vanishing in that region for some parameters, e.g. $M = 2400$ and $Re = 3.0 \times 10^4$. Therefore changes of the mean flow by turbulent momentum transport can be expected to be limited to the side layer regions.

5.5. *The isothermal mean flow*

Figure 21 shows the influence of turbulent momentum transport on the distribution of the streamwise mean velocity $\bar{u}$ in the channel midplane. As the velocity distribution of laminar MHD duct flows is governed by the Hartmann number only, the graphs are presented for constant Hartmann numbers, i.e. $M = 600$ and $M = 4800$. From figure 21 the growing influence of the Reynolds number is clearly demonstrated when the flow becomes time-dependent.

It is clearly seen for the smallest Hartmann number $M = 600$ in figure 21(a) that the turbulent transport of momentum leads to decreasing peak velocities in the sidewall jet. The velocity minimum in the region between the core region and the wall jet disappears while the width of the jet increases. The core region remains at a uniform velocity distribution whose level is slightly increasing with Reynolds number by an enhanced momentum transfer from the side layers. For the strong magnetic field with $M = 4800$ (see figure 21b) the core velocity remains almost unchanged in spite of the increasing Reynolds numbers. In this case turbulent transfer of momentum results in a significant increase of the width of the side layer. The velocity peak in the region close to the wall cannot be measured by the probe because of its limited spatial resolution, but the decrease of the velocity with increasing Reynolds numbers can nevertheless clearly be recognized. Moreover, the minimum of the laminar velocity profile adjacent to the core region seems to move towards the centre of the duct at higher Hartmann numbers. But in the case of highly organized turbulent flow

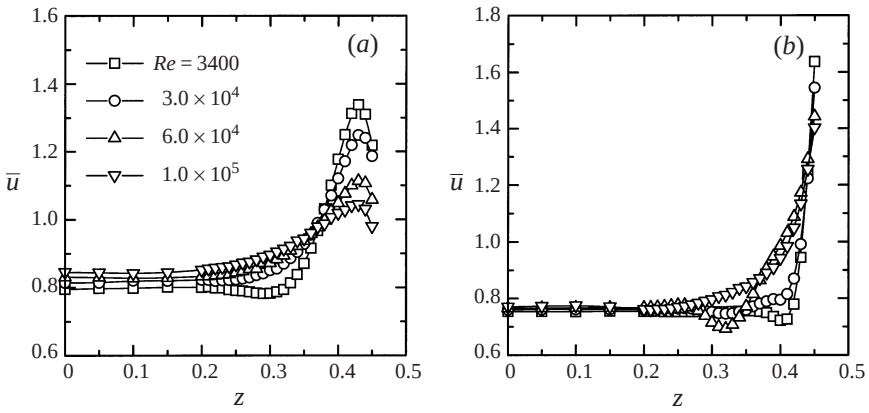

FIGURE 21. Distribution of the mean streamwise velocity $\bar{u}$ in the midplane ($y = 0$). The effect of turbulent momentum transport by increased Reynolds number is shown for Hartmann numbers (*a*) $M = 600$ and (*b*) $M = 4800$.

occurring at $Re = 3.0 \times 10^4$ this minimum is caused by another effect than that for the laminar flow. In fact, it can be identified with the region of upstream fluctuations of the organized vortex pattern along the sidewall. As the mean velocity has been measured only in the midplane of the channel, no direct information on the mean velocity distribution in the direction of the magnetic field is available. Assuming the existence of two-dimensional vortex columns we expect a flattening of the parabolic shape of the laminar sidewall jets.

From an engineering point of view the increase in the pressure drop due to turbulent dissipation is a particular point of interest for any hydraulic design. Tillack (1990) derived an analytical relation for the pressure drop of laminar MHD flow in rectangular ducts with conducting walls for large Hartmann numbers. With the scaling introduced in § 2 this relation is

$$\frac{\partial p}{\partial x} = -\xi = -\frac{M^2}{Re}\left[\frac{1}{3b/a}\frac{\sqrt{M}}{1 + c_S\sqrt{M}} + \frac{1 + c_H}{c_H + 1/M}\right]^{-1}. \tag{5.1}$$

From this relationship, the non-dimensional pressure drop coefficient ξ can be calculated for particular Hartmann and Reynolds numbers. The geometry and the electrical properties of the duct are accounted for by the scaled width b/a and the conductance ratios c_H and c_S. In figure 22 the measured pressure drop coefficient ξ is compared with the predicted pressure drop for laminar flow calculated using relation (5.1).

At constant Hartmann number the pressure drop of laminar flow, denoted by solid lines, is predicted to decay as Re^{-1}. When the Reynolds number is increased beyond the critical value, additional contributions to the pressure drop by dissipation of turbulent kinetic energy should become visible by a less steep decrease of the pressure drop with the Reynolds number in the turbulent regime. Nevertheless, the measurements represented by the symbols agree very well with the calculations given by solid lines in the laminar as well as in the turbulent region. No change in the slope of the laminar flow curve is observed even for the lowest Hartmann number and for high Reynolds numbers.

This result is not surprising because the Reynolds stresses enter the dimensionless momentum equation with a factor $1/N$ with respect to the electromagnetic forces that

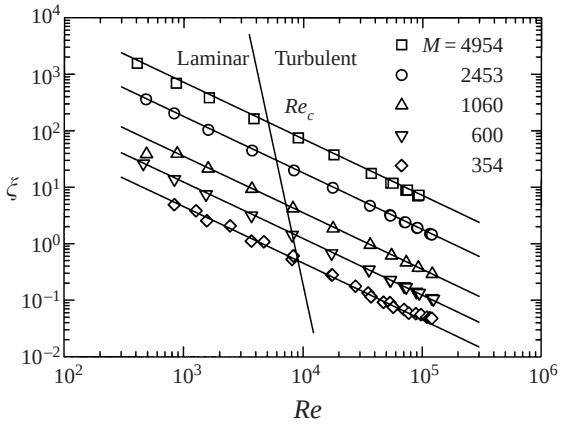

FIGURE 22. Comparison of measured pressure drop coefficients ξ denoted by dots with design predictions assuming laminar MHD flow denoted by solid lines (equation (5.1)).

mainly govern the pressure gradient (see § 2). With N not small a significant increase of the pressure drop cannot be expected.

We conclude that additional pressure losses resulting from dissipation of kinetic energy of Q2D turbulence contribute little to the overall losses in MHD flow originating from Joule's dissipation. Therefore, hydraulic designs for fully developed flow can be carried out by using the laminar pressure relation given by (5.1) to calculate the pressure drop even in turbulent rectangular duct flows.

6. Results for non-isothermal flow

For investigating heat transport phenomena, a heat flux of $15\,\mathrm{W\,cm^{-2}}$ is applied to one sidewall of the test section. The experiments are carried out in the same range of Hartmann and Reynolds numbers as in the case of isothermal flow. In addition, temperature measurements of MHD flows are compared with those of OHD flow indicated by $M = 0$. The Péclet number is evaluated from the Reynolds and Prandtl numbers according to the relation $Pe = Re\,Pr$ with $Pr = 0.03$ for NaK at 60 °C. In the range of strong turbulent flow at $1.5 \times 10^4 < Re < 1.0 \times 10^5$ Péclet numbers in the range $450 < Pe < 3000$ are achieved. With a heated length of $x = 12.5$ the thermal developing length ζ (see § 3.2) is always smaller than unity and thus the flow is far from fully developed thermal conditions.

Because of the layered structure of the flow and the high degree of order in the region of high turbulence intensities, the turbulent transport of heat is expected to be significantly different from OHD flows. To identify the dominant phenomena we first present measurements of local flow quantities and transport properties performed with the help of a traversable probe. The consequences of turbulent heat transport on the heat transfer at the sidewall will be discussed later based on measurements of wall temperatures.

6.1. *The structure of temperature fluctuations*

As the thermal conductivity of liquid metals is very high, disturbances of the temperature field decay fast and, therefore, heat is transported effectively only by large vortices, mixing regions of hot and cold fluid. In figure 23 the time series of the velocity and temperature fluctuations, u' and T' are plotted for a constant Reynolds

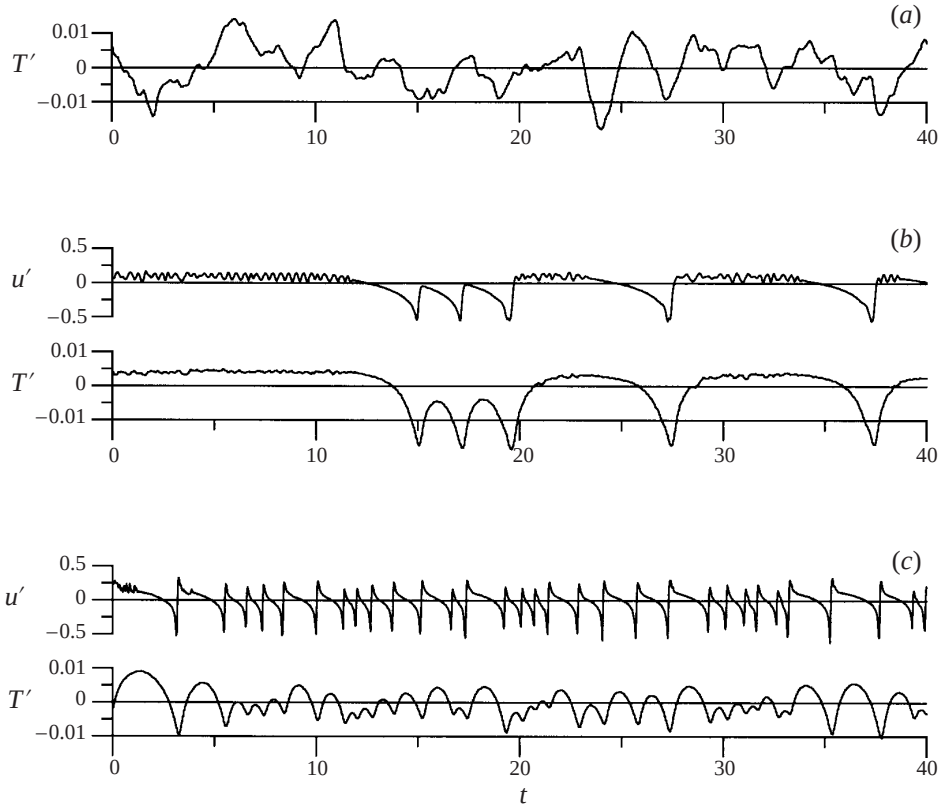

FIGURE 23. Typical time series of the fluctuating part of the streamwise velocity u' and the temperature T'. The probe is located at the near-wall z-position $z = 0.45$. At the Reynolds number $Re = 3.0 \times 10^4$ the Hartmann number is increased from (a) $M = 0$ giving OHD flow to MHD flows at (b) $M = 1200$ and (c) $M = 4800$.

number $Re = 3.0 \times 10^4$. The Hartmann number is increased from an OHD flow with $M = 0$ to MHD flow with $M = 1200$ and $M = 4800$. The probe is located in the midplane and close to the wall at $z = 0.45$.

The time series for the temperature recorded in OHD flow shows a typical random distribution of turbulent fluctuations. Since there is no magnetic field, velocity measurements with the help of potential probes are not possible.

For the Hartmann number $M = 1200$ the time series of the fluctuating velocity u' shows a strong intermittent behaviour. The convective heat transport of large vortices induces distinct disturbances in the temperature field whereas the effect of small-scale velocity perturbations is negligible. At the Hartmann number of $M = 4800$ the turbulence in the side layer is well ordered but the degree of order is not as high as for the isothermal flow shown in figure 13(a). One of the reasons for this effect may be the non-homogeneous physical properties such as viscosity of the liquid metal caused by the temperature gradient in the close wall region. Since the mean flow has been observed to be only weakly changed by this effect this point is not discussed further. The temperature field essentially follows the velocity fluctuations, indicating effective convective transport. But the lack of high-frequency contributions results in an obviously smoother temperature signal. In figure 24 the power spectra of the temperature T and the streamwise velocity component u are compared.

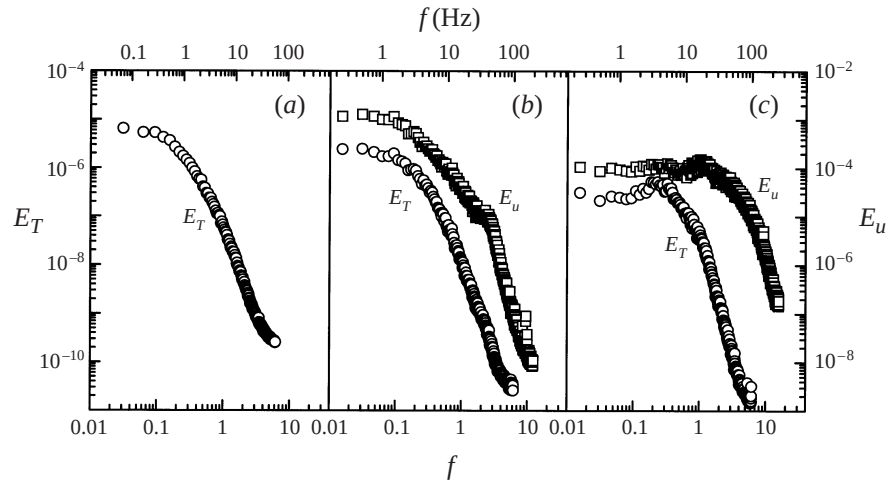

FIGURE 24. Power spectra E_T and E_u of temperature T and streamwise velocity u. At a Reynolds number of $Re = 3.0 \times 10^4$ the Hartmann number is increased from (*a*) OHD flow at $M = 0$ to MHD flows at (*b*) $M = 1200$ and (*c*) $M = 4800$. The probe is located close to the wall at $z = 0.45$.

Increasing the Hartmann number from $M = 1200$ to $M = 4800$ the velocity spectrum is shifted towards higher frequencies. As small-scale fluctuations of the temperature are damped on a fast time scale the temperature field does not follow the fluctuations of the velocity field. The power spectrum of the temperature for $M = 4800$ starts to decrease at a significantly lower cutoff frequency than the velocity spectrum. In figure 24 the dimensional frequency of the spectrum is also shown. As most of the intensity of the temperature power spectrum is concentrated in the frequency range below 50 Hz the temporal resolution of the thermocouples is proven to be adequate for this experiment.

6.2. *Turbulent heat fluxes*

For two-dimensional turbulence with $v' \approx 0$ only the two components perpendicular to the magnetic field $\overline{u'T'}$ and $\overline{w'T'}$ of turbulent heat flux remain non-negligible. These can be measured by the four-electrode probe used. In figure 25 typical distributions of the turbulent heat fluxes are plotted for a *Type I Instability* (see § 5.3) at a low Reynolds number $Re = 1.5 \times 10^4$ and a high Hartmann number $M = 4800$ and for a *Type II Instability* at a high Reynolds number $Re = 1.0 \times 10^5$ and a low Hartmann number $M = 1200$.

For the *Type I Instability* in figure 25(*a*), forming a counter-clockwise rotating vortex street, the distribution of the turbulent heat fluxes can be explained as follows. The positive value of $\overline{u'T'}$ in a thin boundary layer region of about $0.06a$ width indicates turbulent transport of heat in the downstream direction. The negative values of $\overline{w'T'}$ in this range demonstrate the heat flux from the wall towards the core. In the zone adjacent to the laminar core where fluctuations occur mostly in the upstream direction, the vortices are convecting heat upstream and the boundary zone heats up. This induces a reverse turbulent heat transport towards the heated sidewall which is indicated by the positive values of $\overline{w'T'}$ in most of the side layer region.

In spite of the clockwise rotation of vortices for the *Type II Instability* we find positive values of $\overline{u'T'}$ in the near-wall region as well as negative values of $\overline{w'T'}$ (see figure 25*b*). The turbulent flow with low degree of organization causes an intense

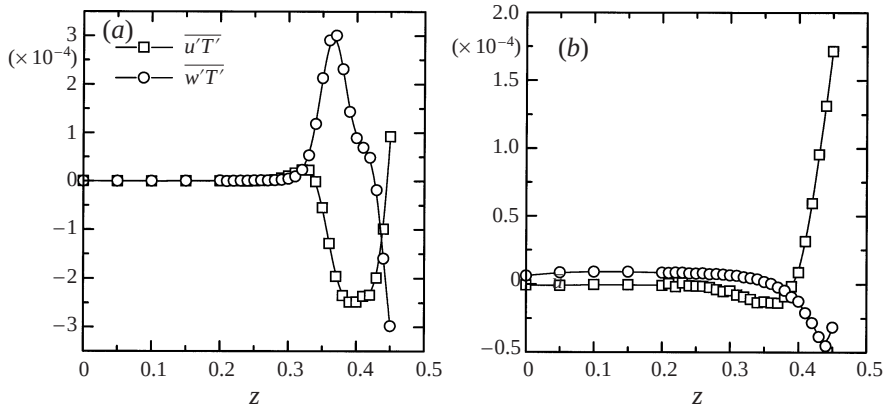

FIGURE 25. Typical distribution of turbulent heat fluxes $\overline{u'T'}$ and $\overline{w'T'}$. (*a*) *Type I Instability* at $Re = 1.5 \times 10^4$ and $M = 4800$. (*b*) *Type II Instability* at $Re = 1.0 \times 10^5$ and $M = 1200$.

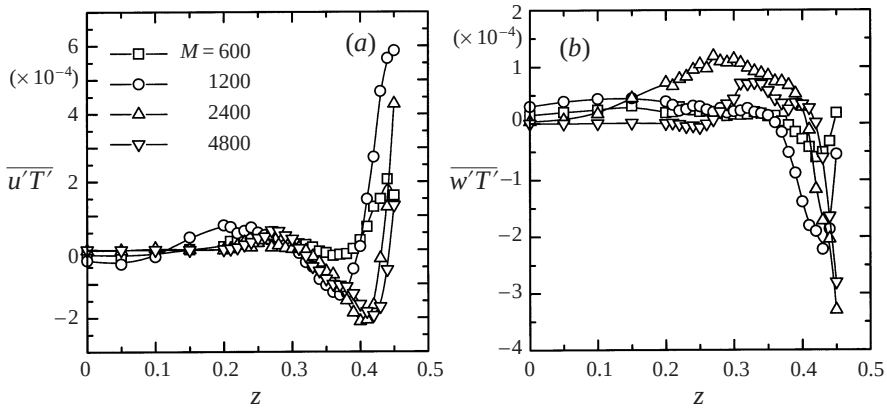

FIGURE 26. The influence of increasing Hartmann number on the distribution of turbulent heat fluxes $\overline{u'T'}$ and $\overline{w'T'}$ in the midplane at constant Reynolds number $Re = 3.0 \times 10^4$.

mixing of hot and cold fluid in the centre part of the side layer. Therefore no reverse heat transfer is observed in the layer.

In figure 26 the influence of increasing Hartmann numbers on the turbulent heat fluxes is shown for $Re = 3.0 \times 10^4$.

The strong changes of the turbulence structure with the Hartmann number complicates the discussion of turbulent heat fluxes. However, an increase of the Hartmann number from $M = 600$ to $M = 2400$ leads to a continuous increase of turbulent heat transport which is indicated by increasing of both $\overline{u'T'}$ and $\overline{w'T'}$. With the further increase of the Hartmann number to $M = 4800$ the turbulent heat fluxes seem to decrease according to the measurements. However the peak values might also be hidden in the near-wall region where they are not accessible for measurements by our probe.

6.3. *The non-isothermal mean flow*

The occurrence of turbulent heat transport may significantly influence the distribution of the mean temperature in the fluid. Developing thermal boundary layers broaden from the turbulent mixing and as a consequence, at a constant wall heat flux boundary condition, the temperature at the heated wall is reduced. Although

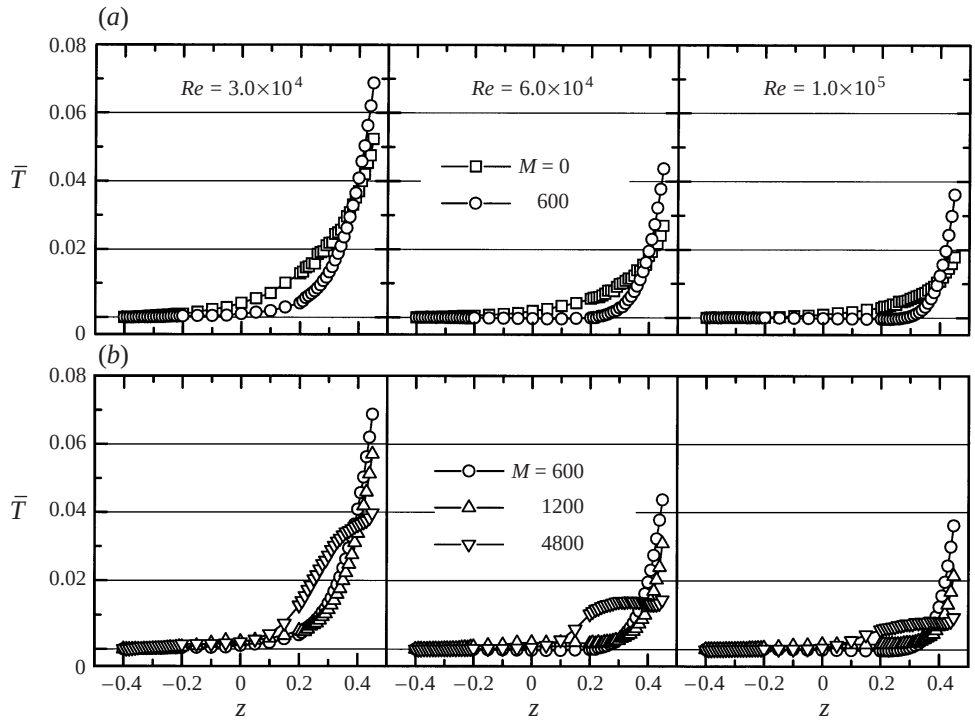

FIGURE 27. Distribution of mean temperature in the midplane after a thermal development length of 12.25*a*. The Reynolds number is fixed to $Re = 3.0 \times 10^4$, $Re = 6.0 \times 10^4$ and $Re = 1.0 \times 10^5$. (*a*) OHD flow ($M = 0$) compared with MHD flow at $M = 600$. (*b*) The effect of higher Hartmann numbers $M = 1200$ and $M = 4800$.

probe measurements are not available up to the fluid–wall interface ($z = 0.5$), lower temperatures in the near-wall region may serve as an indication of better heat transfer at the heated wall.

In figure 27(*a*) the temperature distribution in the midplane at the Hartmann number $M = 600$ is compared with OHD flow ($M = 0$) for the Reynolds numbers $Re = 3.0 \times 10^4$ and $Re = 6.0 \times 10^4$ and $Re = 1.0 \times 10^5$.

The increase of the Reynolds number corresponds to a decrease of the thermal development length (see § 3.2) and therefore the temperature is generally decreased. Simultaneously the width of the thermal boundary layer, i.e. the regions of hot fluid ($\overline{T} > 0$), is decreased. Although significant turbulent heat fluxes have been demonstrated in the previous subsection to occur at $M = 600$ (see figures 26*a* and 26*b*), the temperatures at the heated wall are much higher and the widths of the thermal boundary layers are much smaller than for the OHD flows. Obviously, the effect of Joule's dissipation overrides the effect of turbulence promotion by the magnetic field at this small Hartmann number and therefore the turbulent heat transport at $M = 600$ is significantly lower than in case of OHD flow.

Figure 27(*b*) shows the influence of higher Hartmann numbers $M = 1200$ and $M = 4800$ on the temperature profiles. Decreasing temperature values in the near-wall region at higher magnetic fields clearly indicate an improvement of heat transfer in the sidewall related to increased turbulent heat transport. Moreover, at $M = 1200$ the temperatures in the near-wall region are for all Reynolds numbers already significantly lower than for OHD flow.

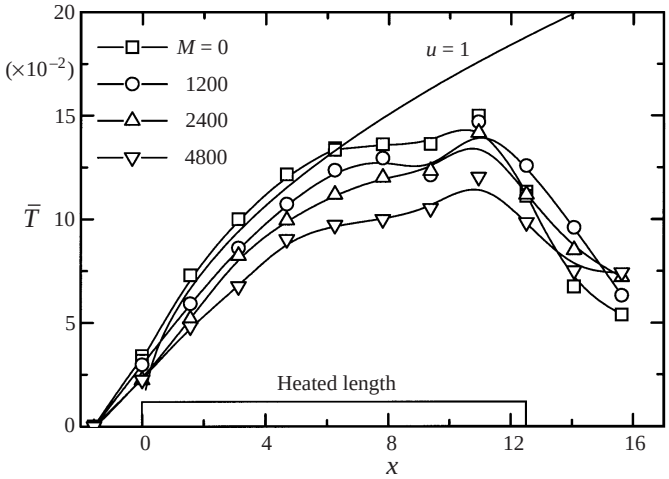

FIGURE 28. Axial development of non-dimensional wall temperatures T_W at $Re = 1.5 \times 10^4$ and increasing Hartmann numbers from OHD flow at $M = 0$ to MHD flow at $M = 4800$. The measurements are compared with a boundary layer solution ($u = 1$) calculated from equation (3.4).

As has been discussed in § 5.4 for the highest Hartmann number $M = 4800$ turbulent velocity fluctuations are confined to the side layer region whereas the core region remains laminar. Heat removed from the wall by the large coherent eddies is transported to an intermediate area between the laminar core and the jet flow where the formation of a laminar purely diffusive thermal boundary layer governs the heat transport into the bulk channel flow. Thus, the turbulent side layer heats up to almost a uniform temperature plateau. At higher Reynolds numbers, e.g. $Re = 6.0 \times 10^4$, the centres of the heat transporting vortices remain colder than the peripheral parts. This can result in an accumulation of heat and a related higher temperature level at the outer boundary of the wall jet. This effect may even lead to a negative mean temperature gradient within the wall jet as it is clearly visible in figure 27(*b*) for the parameter set $Re = 6.0 \times 10^4$ and $M = 4800$. This phenomenon is known as the countergradient heat flux effect since within the individual vortices the heat flux can be transported against the mean driving temperature difference between the wall and the bulk temperature.

6.4. *The development of wall temperatures*

For a uniform wall heat flux boundary condition, the critical spot for the design of a heat transfer unit is always the end of the heated section because of the highest wall temperatures at this location. As in OHD flows the thermal boundary layer develops within a very short distance from the entrance of the heated section into a laminar sublayer of the velocity boundary layer facing the sidewall. The downstream increase of the wall temperature in this region is similar to that of laminar flows. When the thermal boundary layer approaches the turbulent part of the side layer an intense mixing of hot and cold fluid takes place. This turbulent transport of heat will reduce the increase of the wall temperature compared to conditions of laminar flow and the lower wall temperature at a certain entrance length is interpreted as an improvement of heat transfer by turbulent transport.

In figure 28 the influence of increasing Hartmann numbers on the axial development of the temperature at the heated wall is plotted for the Reynolds numbers $Re =$

1.5×10^4. The measurements are taken by thermocouples located in the middle of the heated wall at $y = 0$ (see figure 3*b*). The resolution in the axial flow direction was enhanced by moving the duct with respect to the fixed heater.

The measured values are compared with the solution of the heat transfer equation (3.4) for laminar slug flow. Because of the heat conduction in the sidewall made of stainless steel, the fluid is already slightly heated up when entering the heated section at $x = 0$. At the beginning the temperature increases fast and compares very well with the slug flow solution for T_W. Beyond the entrance length $x \approx 5$ a significant change in the temperature slope is observed which is to be associated with the onset of active mixing in the turbulent side layer. The most important observation is the general decrease of the temperatures at the wall by the enhanced turbulence with increasing Hartmann numbers in the region $2 \leqslant x \leqslant 10$. However, one should be aware of the fact that the formation of high-velocity jets at the heated wall improves heat transfer even without the effect of turbulent transport. Naturally the heat conduction in the sidewall causes the wall temperatures to decrease significantly before the heated section ends at $x = 12.25$, so measured temperature values at positions beyond $x = 10.0$ must be explained as end effects which are not relevant in this context.

7. Concluding remarks

Multipole temperature-potential probes are efficient tools to measure local flow quantities as well as turbulent transport properties in turbulent liquid metal MHD flows. Experimental data have been provided for the integral flow quantities pressure drop and wall temperatures as well as for a number of important details on specific turbulent properties in MHD duct flow. The investigation has been focused on the behaviour of jets in the proximity of the walls parallel to the magnetic field.

In the range of parameters investigated, the turbulent velocity fluctuations are strongly non-isotropic and the observed turbulent flow is quasi-two-dimensional (Q2D). The turbulent flow pattern is dominated by large-scale vortex structures with their axes aligned with the magnetic field, which are convected downstream parallel to the sidewalls. In between the large vortices small-scale turbulent eddy structures occur with a higher degree of isotropy, but their contribution to the turbulent kinetic energy is small. The flow studied is an example in which the magnetic field is enforcing a Q2D structure of turbulence and is simultaneously enhancing the nonlinear processes, which is manifested in the increase of turbulence intensities and Reynolds shear stresses in the proximity of the sidewall.

The first direct measurements of turbulent heat fluxes in MHD flow show that the turbulent heat transport at the walls parallel to the magnetic field is significantly enhanced with the increase of the intensity of the magnetic field. With this benefit of turbulent heat transport, the flow rate in coolant channels of MHD heat transfer units may be significantly reduced compared to design values based on laminar heat transport correlations. Taking into account the negligible contribution of Q2D turbulence to the overall pressure losses, the hydraulic design of piping networks under fully developed MHD conditions can be carried out under the assumption of laminar flow.

The experimental results obtained may form a basis for the development of advanced MHD turbulence models to predict turbulent heat transfer even for larger developing lengths of the thermal boundary layer.

The authors are grateful to Dr L. Bühler and to Dr R. Stieglitz for useful discussions and comments. Special thanks are to Mr K.-J. Mack for unique technical assistance

in performing the experiments. This article is based on the PhD thesis of Ulrich Burr which has been performed at the Institut für Angewandte Thermo- und Fluiddynamik of the Forschungszentrum Karlsruhe.

REFERENCES

Baker, R. C. 1983 A review of recent developments in electromagnetic flow measurement. *Prog. Astronaut. Aeronaut.* **84**, 225–259.

Barleon, L., Mack, K. J., Kirchner, R. & Stieglitz, R. 1996 Heat transfer in MHD-flow at high Hartmann numbers and improvement by turbulence promotion. *Magnetohydrodynamics* **31**, 328–337.

Bühler, L. 1996 Instabilities in quasi-two-dimensional magnetohydrodynamic flows. *J. Fluid Mech.* **326**, 125–150.

Davidson, P. A. 1995 Magnetic damping of jets and vortices. *J. Fluid Mech.* **299**, 153–186.

Evtushenko, I. A., Hua, T. Q., Kirillov, I. R., Reed, C. B. & Sidorenkov, S. S. The effect of a magnetic field on heat transfer in a slotted channel. *Fusion Engng Design* **27**, 587–592.

Kirillov, I. R., Reed, C. B., Barleon, L. & Miyazaki, K. 1995 Present understanding of MHD and heat transfer phenomena for liquid metal blankets. *Fusion Engng Design* **27**, 553–569.

Kit, E. & Tsinober, A. 1971 Possibility of creating and investigating two-dimensional turbulence in a strong magnetic field. *Magnetohydrodynamics* **7**, 312–318.

Kit, L. 1970 Turbulent velocity fluctuation measurements using a conduction anemometer with three-electrode probe. *Magnetohydrodynamics* **6**, 480–484.

Kolesnikov, Y. & Tsinober, A. 1972*a* An experimental study of two-dimensional turbulence behind a grid. *Fluid Dyn.* **9**, 621–624.

Kolesnikov, Y. & Tsinober, A. 1972*b* Two-dimensional flow behind a circular cylinder. *Magnetohydrodynamics* **8**, 300–307.

Oughton, S., Priest, R. & Matthaeus, W. H. 1994 The influence of a mean magnetic field on three- dimensional magnetohydrodynamic turbulence. *J. Fluid Mech.* **280**, 95–117.

Platnieks, I. A. 1972 Correlation study of the transformation of a field of turbulence velocity perturbation in a MHD duct. *Proc. 7th Riga Conf. on MHD*, vol. 1, p. 31.

Reed, C. B. & Picologlou, B. F. 1989 Sidewall flow instabilities in liquid metal MHD-flow under blanket relevant conditions. *Fusion Technol.* **15**, 705–715.

Reed, C. B., Picologlou, B. F., Dauzvardis, P. V. & Bailey, J. L. 1986 Techniques for measurements of velocity in liquid metal MHD-flows. *Fusion Technol.* **10**, 813–821.

Shercliff, J. A. 1962 *The Theory of Electromagnetic Flow-Measurement*. Cambridge University Press.

Shercliff, J. A. 1965 *A textbook of Magnetohydrodynamics.* Pergamon.

Sommeria, J. & Moreau, R. 1982 Why, how and when, MHD turbulence becomes two-dimensional. *J. Fluid Mech.* **118**, 507–518.

Sukoriansky, S. & Branover, H. 1988 Turbulence pecularities caused by interference of magnetic field with energy transfer phenomena. *Prog. Astronaut. Aeronaut.* **112**, 87–99,

Tillack, M. S. 1990 Magnetohydrodynamic flow in rectangular ducts. Design equations for pressure drop and flow quantity. *UCLA-FNT*-41.

Ting, A. L., Walker, J. S., Reed, C. B. & Picologlou, B. F. 1991 Linear stability analysis for high-velocity boundary layers in liquid-metal magnetohydrodynamic flows. *Intl J. Engng Sci.* **29**, 939–948.

Tsinober, A. 1990 MHD Flow drag reduction. *Prog. Astronaut. Aeronaut.* **123**, 327–349.

Tsinober, A., Kit, E. & Teitel, M. 1987 On the relevance of the potential-difference method for turbulence measurements *J. Fluid Mech.* **175**, 447–461.

Zikanov, O. & Thess, A. 1998 Direct numerical simulation of forced MHD turbulence at low magnetic Reynolds number. *J. Fluid Mech.* **358**, 299–333.